

2024

# Modeling and simulations of 2D nano-mechanical resonators

---

<https://hdl.handle.net/2144/48894>

*Downloaded from DSpace Repository, DSpace Institution's institutional repository*

BOSTON UNIVERSITY  
COLLEGE OF ENGINEERING

Thesis

**MODELING AND SIMULATIONS OF  
2D NANO-MECHANICAL RESONATORS**

by

**AMIRREZA REZAEPAZHAND**

B.Sc., Sharif University of Technology, 2022

Submitted in partial fulfillment of the  
requirements for the degree of  
Master of Science

2024



Approved by

First Reader

---

J. Scott Bunch, Ph.D.  
Associate Professor of Mechanical Engineering  
Associate Professor of Materials Science and Engineering  
Associate Professor of Physics

Second Reader

---

J. Gregory McDaniel, Ph.D.  
Associate Professor of Mechanical Engineering  
Associate Professor of Materials Science and Engineering

Third Reader

---

Enrique S. Gutierrez-Wing, Ph.D.  
Master Lecturer in Mechanical Engineering



**MODELING AND SIMULATIONS OF  
2D NANO-MECHANICAL RESONATORS  
AMIRREZA REZAEPAZHAND**

**ABSTRACT**

Nanoelectromechanical systems (NEMS) play an important role in advancing high-precision sensing and high-speed computational applications due to their exceptional sensitivity and reduced size. This thesis explores the dynamic behaviors and vibrational properties of NEMS, focusing on coupled systems of molybdenum disulfide ( $\text{MoS}_2$ ) membrane and silicon nitride ( $\text{SiN}_x$ ) drumhead, and the effects of gas pressure on an  $\text{MoS}_2$  membrane resonator. Employing finite element simulations alongside theoretical modeling, the study thoroughly analyzes the coupling dynamics between  $\text{MoS}_2$  and  $\text{SiN}_x$  resonators and investigates the vibrational responses of  $\text{MoS}_2$  membranes under pressure. Key achievements include the identification of vibrational modes, calculation of coupling constants, and comprehensive understanding of pressurized  $\text{MoS}_2$  membrane resonator behavior. These insights pave the way for enhancing NEMS applications in sensitive detection and resonant frequency modulation, significantly contributing to the field of nanotechnology and the development of advanced NEMS devices.

**Keywords:** Nanoelectromechanical systems,  $\text{MoS}_2$ , Finite element simulation, Coupling constant, Pressurized membranes.

## TABLE OF CONTENTS

ABSTRACT.....	iv
TABLE OF CONTENTS.....	v
LIST OF TABLES.....	vii
LIST OF FIGURES .....	ix
CHAPTER 1. INTRODUCTION.....	1
1.1 Introduction .....	1
1.2 Outline.....	2
1.3 Nano electro-mechanical systems .....	3
1.4 2D materials .....	4
1.5 Molybdenum disulfide .....	7
1.6 Finite Element Analysis .....	9
1.7 COMSOL Multiphysics .....	10
CHAPTER 2. THEORY OF VIBRATION.....	13
2.1 Introduction .....	13
2.2 Vibrations.....	14
2.3 Resonance frequency.....	16
2.4 Nanomechanical resonators.....	18
2.5 2-dimensional vibrations .....	18
2.6 Effective mass .....	21
2.7 Coupled nanomechanical resonators .....	24
2.8 Vibrations of pressurized membrane.....	28

2.9	Derivations of finite element for vibrations .....	31
CHAPTER 3. MODELING OF COUPLED NANORESONATORS .....		34
3.1	Introduction .....	34
3.2	FE simulations of SiN <sub>x</sub> drumhead .....	34
3.3	FE simulations of MoS <sub>2</sub> membrane .....	37
3.4	FE simulations of coupled SiN <sub>x</sub> drumhead and MoS <sub>2</sub> membrane .....	40
3.5	Derivation of method for calculating coupling constant.....	46
3.6	Conclusion.....	53
CHAPTER 4. MODELING OF PRESSURIZED MEMBRANE .....		55
4.1	Introduction .....	55
4.2	Model configuration.....	58
4.3	Tension induced by gas pressure.....	59
4.4	Gas cavity modeled as a spring.....	62
4.5	Coupling between membrane vibration and acoustic resonance .....	64
4.6	Conclusion.....	70
CHAPTER 5. CONCLUSION .....		71
5.1	Summary .....	71
5.2	Future outlook .....	72
BIBLIOGRAPHY.....		74
CURRICULUM VITAE .....		79

## LIST OF TABLES

Table 1 Mechanical properties of graphene versus single layer MoS <sub>2</sub> <sup>28</sup> (Data taken from; Jiang, 2015).....	8
Table 2 Comparison of the effective mass to total mass ratio for a circular membrane across various resonance modes. For each mode, the ratio is determined using the Effective Mass Integral (EMI), calculated both analytically and via finite element analysis <sup>36</sup> (Table taken from; Hauer et al.).....	22
Table 3 Model configuration of annular-shaped silicon nitride drumhead.....	35
Table 4 Mechanical properties of silicon nitride.....	35
Table 5 COMSOL analysis for eight distinct vibrational modes for the annular-shaped silicon nitride drumhead.....	36
Table 6 Model configuration of a circular MoS <sub>2</sub> membrane.....	38
Table 7 Mechanical properties of MoS <sub>2</sub> .....	38
Table 8 COMSOL analysis for eight distinct vibrational modes for the circular MoS <sub>2</sub> membrane.....	39
Table 9 COMSOL analysis for eight distinct vibrational modes for the coupled MoS <sub>2</sub> membrane and silicon nitride drumhead. The setup parameters for both the membrane and drumhead are same as those described in sections 3.2 and 3.3, with the modification that the membrane now has a 10μm × 10 μm square shape.....	43
Table 10 Values for coupling constant calculated through the model proposed.....	52
Table 11 Dimensions and properties of suspended clamped MoS <sub>2</sub> membrane in pressurized membrane models.....	58

Table 12 Dimensions and properties of Argon gas cavity in pressurized membrane models, at 298K.....	58
Table 13 Mode shapes and natural frequencies of acoustic resonance for the cylindrical gas cavity.....	65

## LIST OF FIGURES

Figure 1 NEMS structure with resonance frequency of 21 MHz <sup>8</sup> (Image taken from; Carr et al.).	4
Figure 2 Schematic of suspended graphene nanoresonator <sup>12</sup> (Image taken from; Bunch et al.).	5
Figure 3 Atomic structure of MoS <sub>2</sub> <sup>16</sup> (Figure taken from; Radisavljevic et al.)	7
Figure 4 Resonance of MoS <sub>2</sub> nanoresonator (43.0 nm thickness, 61 layers). The motion of the membrane measured based on the reflection of light waves from the MoS <sub>2</sub> membrane <sup>27</sup> (Figure taken from; Lee et al.)	9
Figure 5 Finite element analysis of deformation of a NEMS pressure sensor with diaphragm structure <sup>31</sup> (Figure taken from; Devi et al.)	10
Figure 6 (a) A one-degree-of-freedom mass-spring system <sup>32</sup> . (b) The motion of the system through time <sup>32</sup> . (Figure taken from; Rao)	15
Figure 7 (a) A one-degree-of-freedom mass-spring system with damping <sup>32</sup> . (b) The motion of the system through time, assuming the damping ratio is less than 1 <sup>32</sup> . (Figure taken from; Rao)	16
Figure 8 a) Image of a suspended graphene membrane with L = 2 μm and W = 3 μm <sup>34</sup> . b) Fundamental resonance mode of the graphene shown in (a). The resonance frequency is equal to 9.77MHz <sup>34</sup> (Figures taken from; Zande et al.)	17
Figure 9 Different 1D and 2D nanomechanical resonators <sup>35</sup> (Figure take from; Xu et al.)	18

Figure 10 Mode shapes of annular plates with fixed boundary conditions on the outer edge and free boundary conditions on the inner edge<sup>37</sup> (Figure taken from; Tornabene et al.).  
..... 21

Figure 11 Schematic of 2-mass-3-spring 2DOF system. The central spring ( $\kappa$ ) links two one-degree-of-freedom (1 DOF) systems (System A and System B), each consisting of a mass ( $m_A$  and  $m_B$ ) and a spring ( $k_A$  and  $k_B$ ), to form a coupled two-degree-of-freedom (2 DOF) system of oscillators. This coupling facilitates the transfer of vibrational energy between the two systems, creating a coupled system<sup>41</sup> (Figure taken from; Novotny). ..... 25

Figure 12 Assuming  $k_A = k_0$  and  $k_B = k_0 + \Delta k$ ; without coupling, the two curves intersect at  $\Delta k = 0$ . With coupling introduced, the curves no longer intersect but exhibit an avoided crossing, indicative of strong coupling<sup>41</sup> (Figure taken from; Novotny). ..... 27

Figure 13 a) Schematic of coupled graphene and silicon nitride nanoresonators<sup>39</sup>. b) Hybridization between graphene and silicon nitride modes;  $\Omega_G$  is the uncoupled graphene mode,  $\Omega_S$  is the uncoupled silicon nitride mode, and  $\Omega_{\pm}$  are the hybridized mode<sup>39</sup> (Figures taken from; Schwarz et al.). ..... 28

Figure 14 a) Schematic of the experimental geometry (side view). b) Simulation geometry in COMSOL..... 42

Figure 15 a) Natural frequencies of the coupled system consisted of SiNx drumhead and MoS<sub>2</sub> membrane plotted versus membrane tension; coupling between modes of MoS<sub>2</sub> and nitride sharing the same mode indices is stronger than coupling between modes with different indices. Each color represents a distinct mode of coupled system. b)

Close-up view of the interaction between the first mode of MoS<sub>2</sub> and the second mode of nitride, showing weak coupling. c) Close-up view of the avoided crossing between the first mode of MoS<sub>2</sub> and the first mode of nitride, highlighting strong coupling... 45

Figure 16 Schematic of a two-mass-three-spring 2 DOF system. .... 47

Figure 17 Curve fitted to the natural frequency data points from COMSOL simulations. The stars represent the data points, and the continuous curve illustrates the fit to these points. Here,  $Z = T_0 - T$ , where  $T_0$  is the initial tension in the membrane, and  $T$  is the tension at the specific frequency being analyzed. The coupling constant determined is 0.0042 N/m, with the error function (resnorm) achieving a value of  $2.2 \times 10^{-6}$ ..... 51

Figure 18 a) Simulated natural frequencies of the coupled system versus tension in the MoS<sub>2</sub>. b) Experimentally measured natural frequencies versus laser power from Yousefi's work (Figure b taken from; Yousefi). Both figures highlight more significant mode splitting, indicative of stronger coupling, between the second mode of MoS<sub>2</sub> and the second mode of silicon nitride compared to the mode splitting between the first mode of MoS<sub>2</sub> and the second mode of silicon nitride. .... 53

Figure 19 Schematic of deformation of membrane due to changes in external pressure, assuming that the internal pressure is constant<sup>42</sup>. (Figure taken from; Yousefi)..... 56

Figure 20 Modeling of the three mechanisms as mass spring harmonic oscillators. a) The first mechanism is the tension induced in the membrane, the sum of this tension and initial tension could be assumed as a spring with  $k_{\text{tension}}$ . b) In addition to the tension, gas in the cavity acts as an spring in the vibration of membrane. c) The third model



includes the coupling between the membrane and acoustic resonance of the gas cavity.

In this case the spring behavior of gas is included in the  $k_{acoustic}$ . ..... 57

Figure 21 Experimental data showing the resonance frequency of a membrane with gas trapped beneath it<sup>42</sup> (Figure taken from; Yousefi). ..... 59

Figure 22 Fundamental natural frequency of the MoS<sub>2</sub> membrane as a function of the pressure difference applied across it, accounting only the tension induced in the membrane based on the deformation. Blue curve shows the simulation result while red curve represents theoretical model based on Hencky’s solution (Eq. 4.x). The MoS<sub>2</sub> membrane features a diameter of 5  $\mu\text{m}$  and a thickness of 6.5  $\text{\AA}$ . ..... 61

Figure 23 Fundamental natural frequency of the MoS<sub>2</sub> membrane as a function of the pressure difference applied across it, in the model with modeling gas as a spring. Blue curve shows the simulation result while red curve represents theoretical model based on energy method solution (Eq. 2.42). The MoS<sub>2</sub> membrane features a diameter of 5  $\mu\text{m}$  and a thickness of 6.5  $\text{\AA}$ . ..... 63

Figure 24 Schematic of the experimental geometry (side view). b) Simulation geometry in COMSOL. .... 67

Figure 25 Resonance modes of the coupled acoustic-membrane system featuring the first three modes. The yellow curve, marked by distinct mode shapes and notable sensitivity to pressure fluctuations, represents the MoS<sub>2</sub> mode within this system. The membrane is a single-layer MoS<sub>2</sub> with a 6.5  $\text{\AA}$  thickness and 5  $\mu\text{m}$  diameter. The cavity is modeled as a cylinder, also with a 5  $\mu\text{m}$  diameter and a depth of 1  $\mu\text{m}$ . ..... 68

Figure 26 Simulation results of the first mode frequency of a pressurized MoS<sub>2</sub> membrane:  
the green curve represents the membrane coupled with the acoustic resonance of the  
gas cavity, and the blue curve represents the membrane without acoustic coupling. The  
membrane has a diameter of 5  $\mu\text{m}$ , and the gas cavity beneath it has a depth of 1  $\mu\text{m}$ .

..... 69

## CHAPTER 1. INTRODUCTION

### 1.1 Introduction

In the fast-growing field of nanotechnology, exploring nanoelectromechanical systems (NEMS) leads to remarkable applications like sensitive detectors and high-speed resonators. Specifically, two-dimensional (2D) materials, especially molybdenum disulfide ( $\text{MoS}_2$ ) have gained significant attention due to their unique mechanical and electronic properties, including high tensile strength, flexibility, and a semiconducting behavior with a direct bandgap. These materials are changing how we design and make NEMS devices, enhancing their performance significantly. Understanding the vibrational dynamics of these materials is essential for improving nanoresonator NEMS devices.

This thesis is motivated by the potential of  $\text{MoS}_2$  membranes to advance the capabilities of NEMS through their coupling with  $\text{SiN}_x$  drumhead and interaction with gas pressure. Coupling NEMS nanoresonators may enhance their performance, such as increasing sensitivity in detecting forces<sup>1</sup>. Moreover, deploying arrays of coupled nanoresonators could offer an approach for creating mechanical-based processing units<sup>2</sup>. Additionally, atomically thin membranes under pressure are well-suited for use in pressure sensor applications<sup>3</sup>.

Previous studies in our group involved both experimental and theoretical studies on coupled nanoresonators and pressurized  $\text{MoS}_2$  membranes. However, this work had limitations in terms of numerical simulation efforts.

The objectives of this thesis have two main parts: firstly, to investigate the dynamic behavior of MoS<sub>2</sub> membrane and SiN<sub>x</sub> drumhead in coupled configurations, explaining the mechanics behind these novel NEMS devices; and secondly, to investigate the effects of gas pressure on the vibrational characteristics of MoS<sub>2</sub> membranes. Through detailed finite element simulation studies and the development of a theoretical model for estimating the coupling constant of two coupled nanoresonators, this work aims to contribute valuable knowledge to the field of nanotechnology and prepare for the development of future NEMS devices.

## 1.2 Outline

This thesis investigates finite element simulations of a coupled MoS<sub>2</sub> membrane and SiN<sub>x</sub> drumhead, alongside simulations of a pressurized MoS<sub>2</sub> membrane interacting with argon gas. The aim is to investigate the vibrational behavior of these nanoelectromechanical systems (NEMS). It also presents a theoretical model for estimating the coupling constant of two coupled nanoresonators. Chapter 1 provides a comprehensive overview of fundamental concepts relevant to the study. Chapter 2 outlines the theoretical models and analytical approaches necessary for interpreting the results of the simulations. Chapter 3 details the outcomes of the simulations involving the coupled MoS<sub>2</sub> membrane and SiN<sub>x</sub> drumhead, including a thorough examination of the results. This section also introduces the derivation of a model for the coupling constant, informed by the insights gained from the simulations. Chapter 4 presents simulations of a pressurized MoS<sub>2</sub> membrane coupled with the acoustic pressure of argon gas, highlighting their interactions.

Chapter 5 consists of a summary of the whole thesis and possible future outlook on this research.

### **1.3 Nano electro-mechanical systems**

Nanoelectromechanical systems (NEMS) represent a key improvement in the miniaturization of mechanical and electrical systems, extending the capabilities of microelectromechanical systems (MEMS) into the nanometer scale. The transition to such a scale enhances performance characteristics, including reduced power requirements and increased sensitivity<sup>4</sup>.

NEMS have the potential to revolutionize several fields. In healthcare, they could lead to new diagnostic tools that detect diseases with high precision<sup>5</sup>. In computing, they offer the possibility of creating components that operate on less power, making devices more efficient<sup>6</sup>. Additionally, NEMS resonators, characterized by their high quality factor (Q), can be utilized to develop ultrafast sensors, and signal processing units<sup>7</sup>.

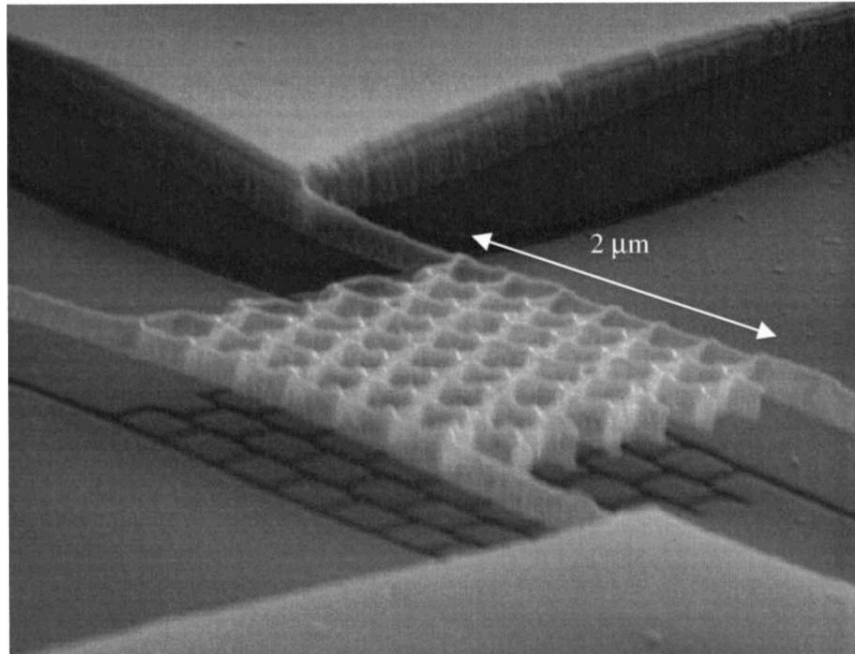


Figure 1 NEMS structure with resonance frequency of 21 MHz<sup>8</sup> (Image taken from; Carr et al.).

Fabrication techniques for NEMS are rooted in advanced fabrication methods, such as electron-beam lithography, chemical vapor deposition(CVD), and lift-off methods, which allow for the precise construction of nanoscale components. These methods have been instrumental in overcoming the challenges associated with scaling down device size, thus enabling the practical realization of NEMS<sup>9</sup>.

#### **1.4 2D materials**

Nanomaterials are materials that at least one of their dimensions is at the nanometer scale. Two-dimensional (2D) materials are a class of nanomaterials that consist of a single layer, or a few layers of atoms arranged in a two-dimensional pattern. These materials exhibit unique physical, chemical, and electronic properties that differ significantly from their bulk corresponding parts due to their extreme thinness and high surface area<sup>10</sup>. Since

the discovery of graphene<sup>11</sup>, a single layer of carbon atoms arranged in a hexagonal lattice, the field of 2D materials has expanded rapidly to include a wide variety of materials, including transition metal dichalcogenides (TMDs), hexagonal boron nitride (h-BN), and black phosphorus (BP).

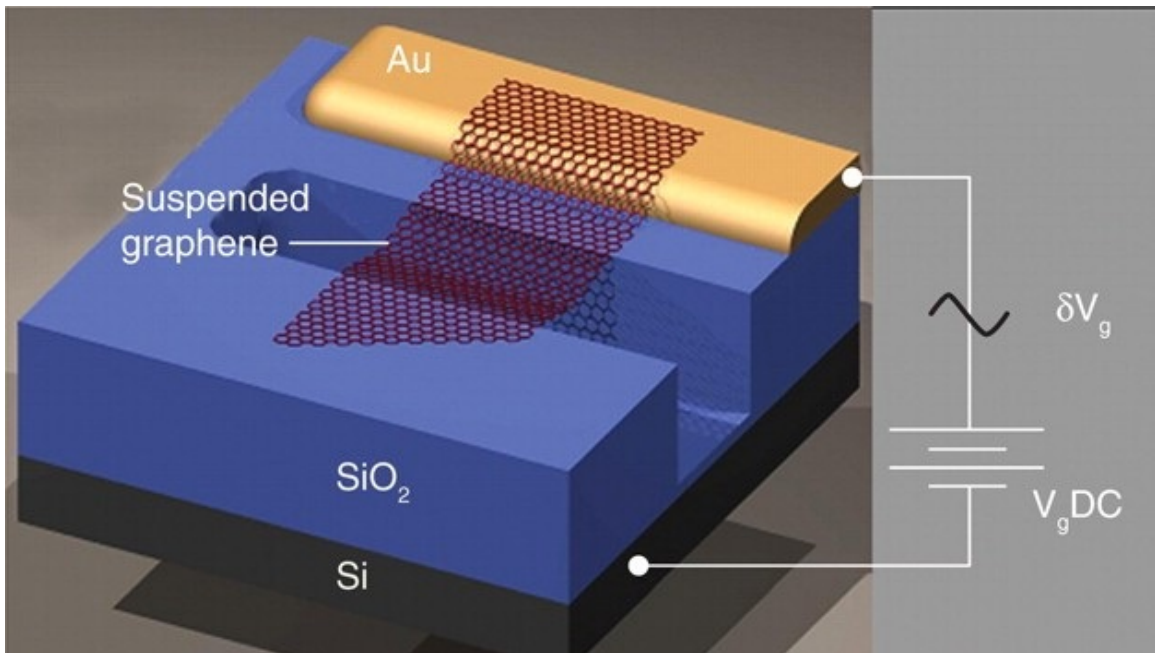


Figure 2 Schematic of suspended graphene nanoresonator<sup>12</sup> (Image taken from; Bunch et al.).

The applications of two-dimensional (2D) materials extend across a wide range of fields, because of their unique electronic, mechanical, optical, and chemical properties. These materials have opened up new possibilities in electronics, photonics, energy storage and conversion, sensing, and biomedicine.

Graphene, due to its exceptional electrical conductivity, mechanical strength, and thermal conductivity, has been the subject of extensive research and is considered a revolutionary material for applications in electronics<sup>13</sup>, energy storage<sup>14</sup>, and biomedical engineering<sup>15</sup>.

Beyond graphene, TMDs like MoS<sub>2</sub> and WSe<sub>2</sub> are semiconductors with tunable band gaps that make them suitable for electronic and optoelectronic applications, such as transistors<sup>16</sup>, photodetectors<sup>17</sup>, electroluminescent devices<sup>18</sup>, and light-emitting diodes (LEDs)<sup>19</sup>.

Hexagonal boron nitride, with its wide band gap, serves as an excellent insulating layer in 2D electronic devices, while black phosphorus is noted for its tunable bandgap depending on its layer thickness, making it promising for photonic and electronic devices<sup>20</sup>.

The synthesis of 2D materials can be achieved through various methods, including mechanical exfoliation, chemical vapor deposition (CVD), and chemical exfoliation, each method offering a different balance between quality, scalability, and cost. Mechanical exfoliation, while simple, typically produces small flakes suitable for fundamental studies rather than large-scale applications. In contrast, CVD can produce large-area films of 2D materials, making it more suitable for various applications<sup>21,22</sup>.

The integration of 2D materials into nanoelectromechanical systems (NEMS) has opened up new possibilities for creating devices with unprecedented performance and functionality. The mechanical strength, coupled with the electrical and optical properties of 2D materials, enables the fabrication of highly sensitive, robust, and versatile NEMS devices<sup>23,24</sup>. Such devices have found applications in high-precision sensors, actuators, and resonators, where the reduced dimensionality and high surface-to-volume ratio of 2D materials lead to very high natural frequency and rich nonlinear dynamics behavior and tunable electronic properties<sup>25</sup>. Among these, MoS<sub>2</sub> nano-resonators stand out for their



exceptional mechanical and electronic properties, offering high resonance frequencies and quality factors, which are critical for ultra-sensitive detection and high-speed nanomechanical computing applications. The unique semiconducting nature of MoS<sub>2</sub>, combined with its mechanical resilience, makes it an ideal candidate for next-generation NEMS resonators<sup>10,26,27</sup>.

### 1.5 Molybdenum disulfide

Molybdenum disulfide (MoS<sub>2</sub>) is a semiconducting member of the transition metal dichalcogenides (TMDs) family, known for its layered structure with a single layer of molybdenum atoms sandwiched between two layers of sulfur atoms (Figure 3).

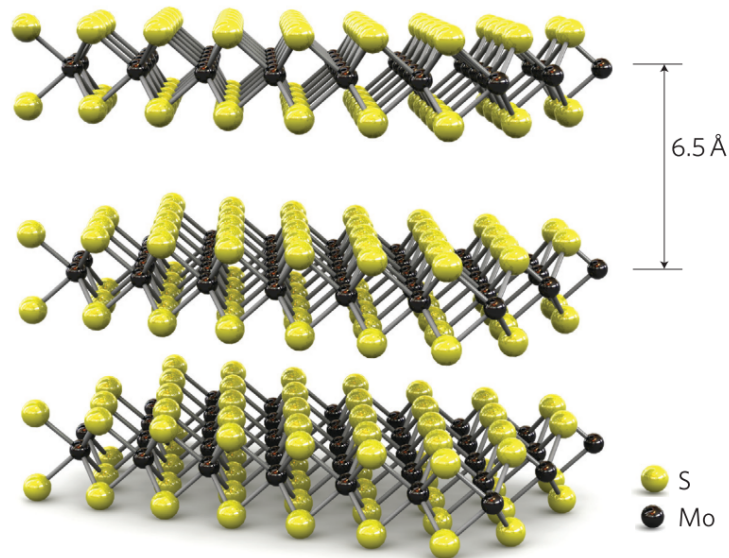


Figure 3 Atomic structure of MoS<sub>2</sub><sup>16</sup> (Figure taken from; Radisavljevic et al.)

MoS<sub>2</sub> has been demonstrated to possess strong mechanical properties, with an in-plane stiffness of approximately 180 N/m, equating to an effective Young's modulus of 270

GPa<sup>28</sup> (Jiang, 2015). While its mechanical strength may not be as good as graphene's, it remains sufficiently strong for use in flexible electronics and optoelectronics (Table 1). Unlike graphene, MoS<sub>2</sub> possesses a bandgap, which enables its use in electronic and optoelectronic applications where semiconducting properties are essential. This bandgap, variable based on the number of layers, shifting from a 1.2 eV indirect gap in bulk to a 1.9 eV direct gap in a single layer<sup>29</sup>, allows for the tuning of electronic and optical properties, making MoS<sub>2</sub> a useful material for a wide range of applications in photodetectors<sup>17</sup>, light-emitting diodes (LEDs)<sup>19</sup>.

Properties	Graphene	Single layer MoS <sub>2</sub>
Young's modulus	$E^{2D} = 335.0 \text{ N}\cdot\text{m}^{-1}$	$E^{2D} = 120 - 180 \text{ N}\cdot\text{m}^{-1}$
Yield stress	$\sigma_{\text{int}} = 42 - 44.4 \text{ N}\cdot\text{m}^{-1}$	$\sigma_{\text{int}} = 15 - 17.5 \text{ N}\cdot\text{m}^{-1}$
Nanoresonator	$f_0 \times Q = 6.4T^{-1.2} \times 10^3 \text{ THz}$	$f_0 \times Q = 2.4T^{-1.3} \times 10^4 \text{ THz}$
Thermal conductivity	$60 \text{ W}\cdot\text{m}^{-1}\cdot\text{K}^{-1}$ (L = 10 nm) $250 \text{ W}\cdot\text{m}^{-1}\cdot\text{K}^{-1}$ (L = 300nm)	$6\text{W}\cdot\text{m}^{-1}\cdot\text{K}^{-1}$ (L = 4 nm) $2\text{W}\cdot\text{m}^{-1}\cdot\text{K}^{-1}$ (L = 120 nm)
Electronic band	$E_{\text{gap}} = 0$	$E_{\text{gap}} \approx 1.8 \text{ eV}$ (direct)

Table 1 Mechanical properties of Graphene versus Single layer MoS<sub>2</sub><sup>28</sup> (Data taken from; Jiang, 2015)

MoS<sub>2</sub> exhibits unique vibrational properties that are critical for its role as a nanoresonator. Its inherent stiffness combined with the low mass of the resonator, makes MoS<sub>2</sub>-based nanoresonators extremely sensitive to changes in displacements, making them ideal for applications in sensing at the molecular level. The ability of MoS<sub>2</sub> nanoresonators to operate at high frequencies with their low mass is particularly advantageous for the development of ultra-sensitive displacement detection systems<sup>27</sup>.

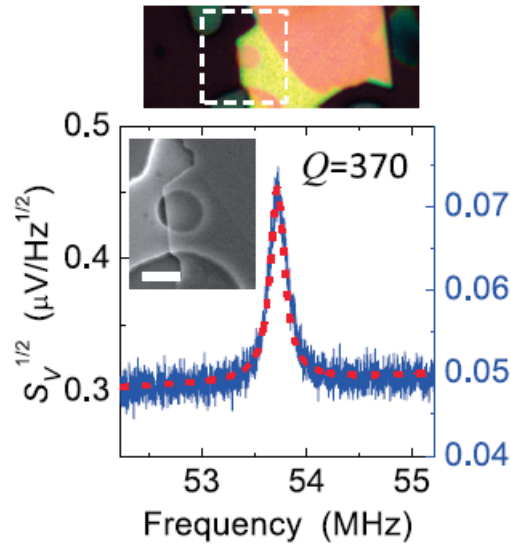


Figure 4 Resonance of MoS<sub>2</sub> nanoresonator (43.0 nm thickness, 61 layers). The motion of the membrane measured based on the reflection of light waves from the MoS<sub>2</sub> membrane<sup>27</sup> (Figure taken from; Lee et al.)

Moreover, the importance of MoS<sub>2</sub> extends beyond electronic and mechanical applications. Its chemical stability, high mechanical strength, and flexibility enable its use in flexible electronics, energy storage devices, and even as a catalyst in hydrogen evolution reactions<sup>30</sup>.

### 1.6 Finite Element Analysis

The finite element method (FEM) is a common approach for the numerical solution of differential equations in the fields of engineering and physics. It is frequently used in various areas such as structural analysis, fluid dynamics, heat transfer, etc.

FEM operates by breaking down a complex system into smaller, manageable parts known as elements. Through this approach, space is discretized by the construction of a mesh over the system, creating a defined numerical domain with a finite number of solution

points. The method then approximates the unknown function across the domain, transforming the problem into a set of algebraic equations.

These simpler equations generated for each element are compiled into a larger equation system that models the entire problem. FEM seeks an approximate solution by minimizing an associated error function, utilizing variational calculus. This analytical process using FEM is commonly referred to as finite element analysis (FEA).

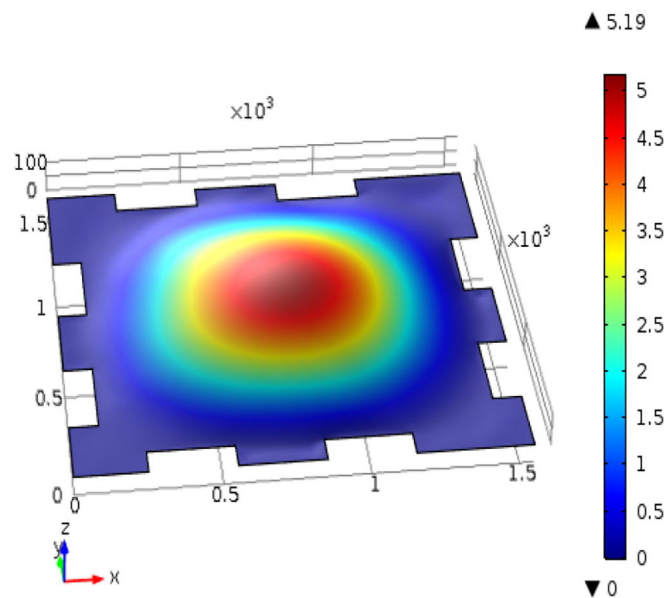


Figure 5 Finite element analysis of deformation of a NEMS pressure sensor with diaphragm structure<sup>31</sup> (Figure taken from; Devi et al.)

## 1.7 COMSOL Multiphysics

COMSOL Multiphysics is a powerful simulation software that provides tools for modeling and solving all kinds of scientific and engineering problems, especially those involving multiphysics phenomena. It integrates seamlessly various physics-based models, making it a valuable tool for researchers and engineers working in fields ranging from

acoustics and electromagnetics to fluid dynamics and structural mechanics. COMSOL Multiphysics performs the simulation of complex systems by solving differential equations that describe physical processes by finite element, enabling users to visualize and predict the behavior of real-world systems.

One of the capabilities of COMSOL Multiphysics is its application in the vibrational analysis of 2D materials. As previously mentioned, 2D materials, such as graphene and transition metal dichalcogenides (TMDs), have attracted significant interest due to their unique electronic, mechanical, and optical properties. Vibrational analysis, particularly through modal analysis and eigenfrequency studies, is crucial for understanding the dynamic behavior of these materials under various conditions.

Using COMSOL Multiphysics for vibrational analysis of 2D materials allows us to explore the effects of mechanical strain, and material interfaces on the vibrational modes of these ultra-thin structures. Such simulations can provide insights into the material properties such as resonance frequencies, and quality factors, which are essential for designing devices based on 2D materials.

COMSOL's simulation capabilities extend to the analysis of hybrid systems, where 2D materials are integrated with solid substrates or interact with gas environments. This coupling is particularly relevant in the development of advanced sensors, actuators, and energy devices, where the interface between different materials plays a crucial role in device performance.

By enabling the detailed simulation of these complex interactions, COMSOL Multiphysics plays a key role in advancing the understanding and application of 2D materials in conjunction with solid materials and gas environments.

## CHAPTER 2. THEORY OF VIBRATION

### 2.1 Introduction

This chapter explores the foundational concepts of vibrations, where we examine the oscillatory motions that occur around an equilibrium point. We introduce the basic dynamics of a one-degree-of-freedom mass-spring system, both undamped and damped, to illustrate the principles of free oscillation and the effects of damping on system behavior. This leads to a discussion on resonance, where a system oscillates at maximum amplitude when driven by an external force at its natural frequency. The focus then shifts to the vibrations of nanomechanical resonators, exploring the distinct behaviors of two-dimensional resonators, including rectangular, circular, and annular membranes.

A portion of this chapter is dedicated to the concept of effective mass, an essential parameter in the dynamics of resonators such as membranes. Effective mass is the portion of a resonator's total mass that actively participates in vibrational motion. This concept becomes especially important in the context of nanomechanical resonators, where the vibrational mode shape significantly influence the effective mass.

Moreover, the chapter expands on the topic of coupled vibrations, emphasizing how nanomechanical resonators interact within coupled systems. The behavior of these coupled systems is investigated using the principles of coupled harmonic oscillators, revealing the complex interactions that develop between them.

Ending with an overview of FEM for analyzing vibrations and coupled systems, this chapter prepares us for a more detailed look at the vibration-related phenomena crucial

for designing and understanding both large-scale and nanoscale mechanical systems.

## 2.2 Vibrations

Vibration, or oscillation, refers to any repeated movement around an equilibrium point, like the vibration of a drum skin when struck. The theory of vibration examines the oscillatory movements of objects and the forces related to them<sup>32</sup>.

Vibration is characterized by the continuous exchange between potential energy and kinetic energy. Thus, a vibrating system requires two key elements: one to hold potential energy and another to hold kinetic energy. These elements are known as the spring or elastic element, which stores potential energy, and the mass or inertia element, which stores kinetic energy. In each cycle of movement, the elastic element transfers its stored potential energy to the inertia element as kinetic energy, and this process reverses, maintaining the cycle of vibration<sup>32</sup>.

To further illustrate, consider a one-degree-of-freedom undamped mass-spring system (figure 6). The governing equation for such a system would be as follows:

$$m\ddot{x} + kx = f(t) \quad (2.1)$$

where  $m$  is the mass,  $k$  is the stiffness, and  $f$  is the external force. This equation results from examining the forces acting on the system. In the absence of external forces, the resonator will oscillate freely, and the governing equation will be as follows:

$$m\ddot{x} + kx = 0 \quad (2.2)$$



By solving this ordinary differential equation (ODE), the motion of the resonator can be described as follows:

$$x(t) = X \cos(\omega_n t - \phi) \quad (2.3)$$

Where  $\omega_n$  is the natural frequency of the system.

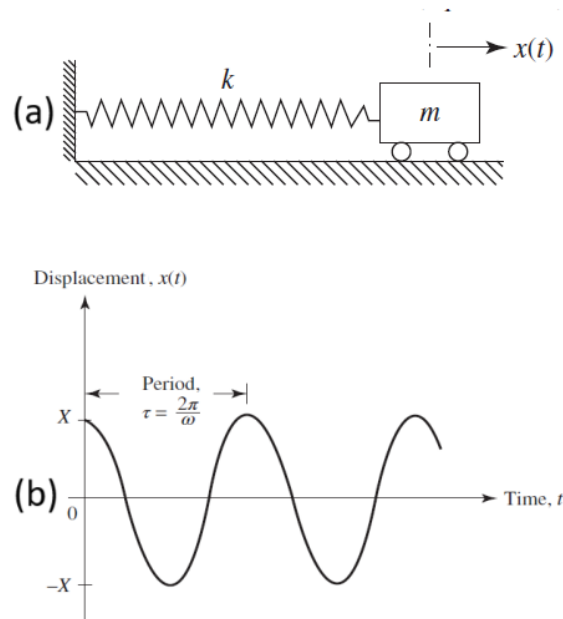


Figure 6 (a) A one-degree-of-freedom mass-spring system<sup>32</sup>. (b) The motion of the system through time<sup>32</sup>. (Figure taken from; Rao)

Introducing viscous damping modifies the free oscillating governing equation to:

$$m\ddot{x} + c\dot{x} + kx = 0 \quad (2.4)$$

which could be rewritten as:

$$\ddot{x} + 2\zeta\omega_n \dot{x} + \omega_n^2 x = 0 \quad (2.5)$$

$$\zeta = \frac{c}{2m\omega_n} \quad (2.6)$$

In which  $\zeta$  is the damping ratio. The system is classified as underdamped, critically damped, or overdamped based on whether the damping ratio is less than 1, exactly 1, or

greater than 1, respectively. If the system is critically damped or overdamped, it will not oscillate. Therefore, what is required here is the equation of motion for a system with a damping ratio below 1, which can be represented as follows:

$$x(t) = e^{-\zeta\omega_n t} \left( x_0 \cos\omega_d t + \frac{\dot{x}_0 + \zeta\omega_n x_0}{\omega_d} \sin\omega_d t \right) \quad (2.7)$$

$$\omega_d = \omega_n \sqrt{1 - \zeta^2} \quad (2.8)$$

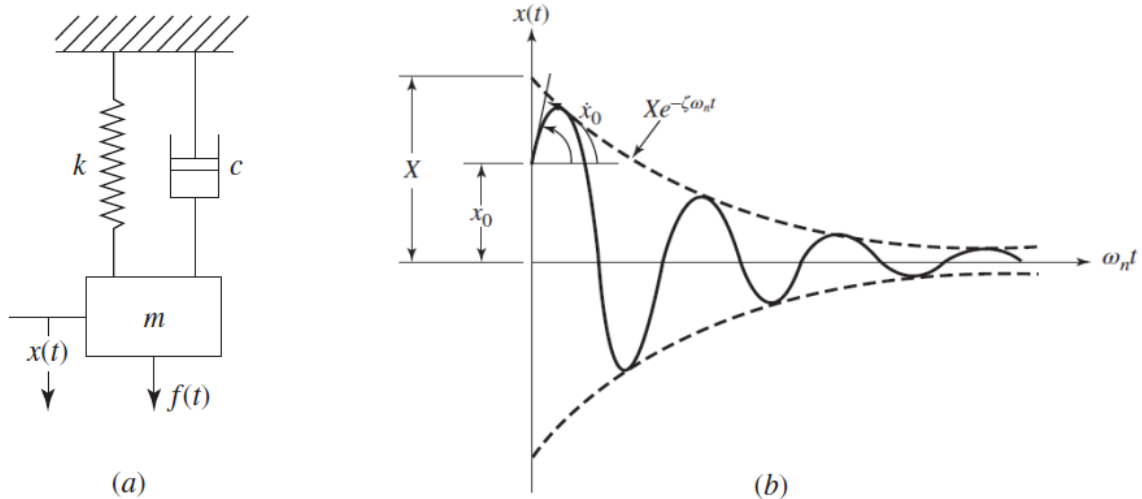


Figure 7 (a) A one-degree-of-freedom mass-spring system with damping<sup>32</sup>. (b) The motion of the system through time, assuming the damping ratio is less than 1<sup>32</sup>. (Figure taken from; Rao)

### 2.3 Resonance frequency

Resonance is a phenomenon observed across various physical systems, where a system vibrates at maximum amplitude under the influence of an external force that matches the system's natural frequency<sup>33</sup>. This principle is establishing in mechanical, acoustic, electrical, and optical systems.

In a mechanical context, resonance occurs when an oscillating force drives another system to oscillate with greater amplitude at a specific frequency, known as the resonant

frequency. This is the frequency at which the system naturally oscillates in the absence of damping or driving forces.

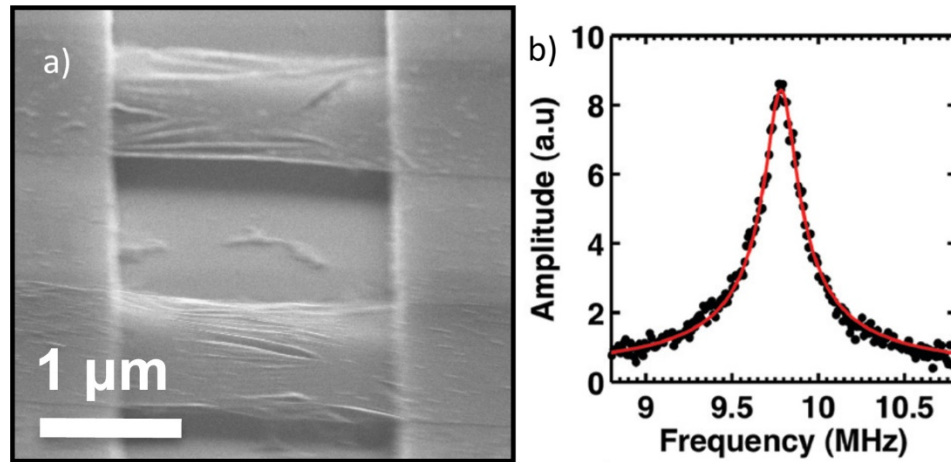


Figure 8 a) Image of a suspended graphene membrane with  $L = 2 \mu\text{m}$  and  $W = 3 \mu\text{m}$ <sup>34</sup>. b) Fundamental resonance mode of the graphene shown in (a). The resonance frequency is equal to  $9.77\text{MHz}$ <sup>34</sup> (Figures taken from; Zande et al.).

In a perfect mechanical system without energy loss, vibrating at its natural frequency, the kinetic energy associated with a particular mechanical oscillation equals the potential energy stored due to the structural deformation caused by the vibration. These systems have many vibration patterns, called eigenmodes, showing this energy balance. At natural frequencies, the system keeps swapping energy between kinetic and potential energy. So, if you give the system a push, it will keep vibrating at this special frequency with a stable amplitude of oscillation<sup>33</sup>.

To find these vibration patterns in structures like beams or strings, we use motion equations, ensuring all forces balance out. This way, we can solve for many simple structures. But with some shapes, like membranes, it gets hard to solve these equations. Then, we predict the vibration patterns based on energy concepts<sup>33</sup>.

## 2.4 Nanomechanical resonators

Nanomechanical resonators consist of continuous mechanical configurations, including beams, strings, or membranes. These devices operate at the nanoscale, employing the unique properties of materials at this scale to perform mechanical vibrations<sup>33</sup>. Typically, nanomechanical resonators are categorized into two types: one-dimensional resonators and two-dimensional resonators<sup>35</sup> (Figure 9).

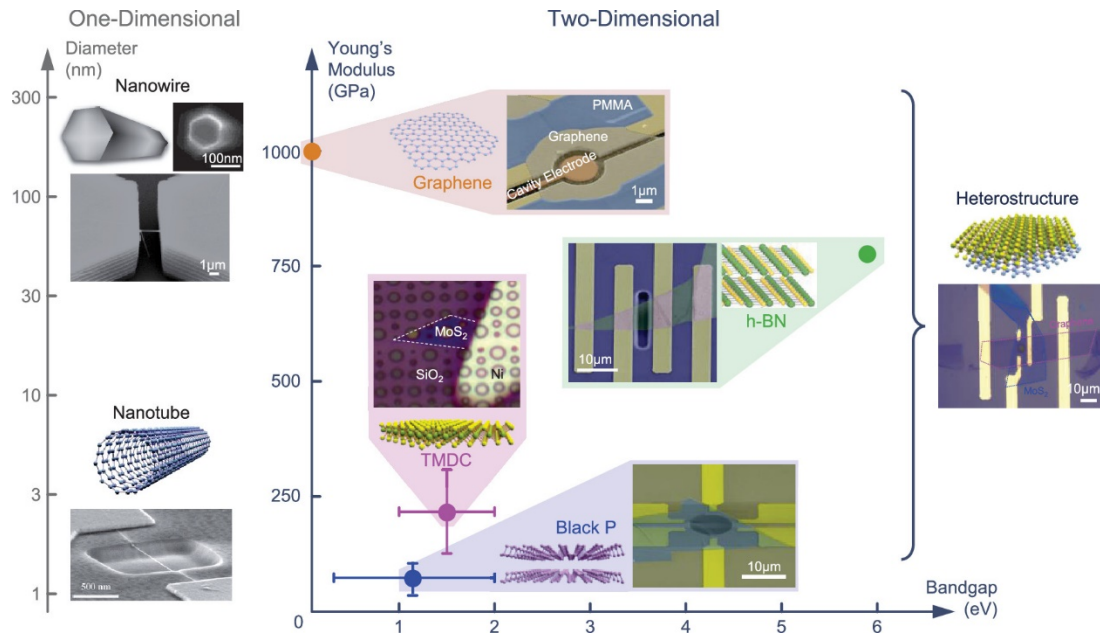


Figure 9 Different 1D and 2D nanomechanical resonators<sup>35</sup> (Figure take from; Xu et al.).

## 2.5 2-dimensional vibrations

Two-dimensional (2D) vibrations and resonances are critical phenomena in the study of mechanical systems, particularly in the analysis of thin structures like membranes and plates. These structures exhibit unique vibrational behaviors due to their geometry,

leading to specific resonance patterns when subjected to external forces. In this section, we will take a closer look at the vibrations of rectangular, circular, and annular membranes.

### 2.5.1 *Vibration of rectangular membranes*

The vibrational patterns, or modes, of rectangular membranes are derived from the equation of motion, which is based on the two-dimensional wave equation<sup>36</sup>:

$$\frac{\partial^2 z}{\partial x^2} + \frac{\partial^2 z}{\partial y^2} - \frac{\rho}{\sigma} \frac{\partial^2 z}{\partial t^2} = 0 \quad (2.9)$$

The modes are determined by solving this equation with boundary conditions that match how the membrane is supported<sup>36</sup>:

$$z(x, y, t) = \sum_m \sum_n a_{mn}(t) \psi_{mn}(x, y) \quad (2.10)$$

in which  $\psi_{mn}$  is the normalized mode shape. By implementing fixed boundary conditions along the edges of the rectangular membrane, the normalized mode shape can be expressed as follows<sup>36</sup>:

$$\psi_{mn}(x, y) = \sin\left(\frac{\pi m x}{L_x}\right) \sin\left(\frac{\pi n y}{L_y}\right) \quad (2.11)$$

where  $L_x$  and  $L_y$  denote the dimensions of the rectangular membrane. Determining the eigenfrequencies of vibrations in this case relies on Rayleigh's principle, resulting in the eigenfrequencies being expressed as follows<sup>33</sup>:

$$\omega_{m,n} = \sqrt{\frac{\sigma}{\rho}} \sqrt{\frac{m^2 \pi^2}{L_x^2} + \frac{n^2 \pi^2}{L_y^2}} \quad (2.12)$$

### 2.5.2 Vibration of circular membranes

Circular membranes exhibit radial symmetry in their vibrational modes. These modes are described by Bessel functions, reflecting the membrane's geometry and boundary conditions. The equation of motion can be represented as follows<sup>36</sup>:

$$\nabla^2 z - \frac{\rho}{\sigma} \frac{\partial^2 z}{\partial t^2} = 0 \quad (2.13)$$

Solving this equation within cylindrical coordinates results in<sup>36</sup>:

$$z(s, \varphi, t) = \sum_m \sum_n a_{mn}(t) \psi_{mn}(s, \varphi) \quad (2.14)$$

In which  $\psi_{mn}$  is the normalized mode shape, based on the Bessel function. By implementing fixed boundary conditions along the edges of the circular membrane, the normalized mode shape can be expressed as follows<sup>36</sup>:

$$\psi_{mn}(s, \varphi) = K_m \cos(m\varphi) J_m\left(\frac{\alpha_{mn}s}{a}\right) \quad (2.15)$$

Where  $J_m$  denotes the Bessel function,  $K_m$  is a constant that normalizes the maximum value of  $\psi$  to equal 1,  $a$  is the radius of the membrane, and  $\alpha_{mn}$  is the  $n^{\text{th}}$  root of the  $J_m$ . The determination of eigenfrequencies is based on Rayleigh's principle, which yield the eigenfrequencies as follows<sup>33</sup>:

$$\omega_{m,n} = \frac{\alpha_{mn}}{a} \sqrt{\frac{\sigma}{\rho}} \quad (2.16)$$

### 2.5.3 Vibration of annular membranes

Annular membranes, which are circular membranes with a central hole, present a more complex case for vibrational analysis due to the additional boundary introduced by the hole. The first 10 resonant mode shapes of an annular plate are depicted in Figure 10.

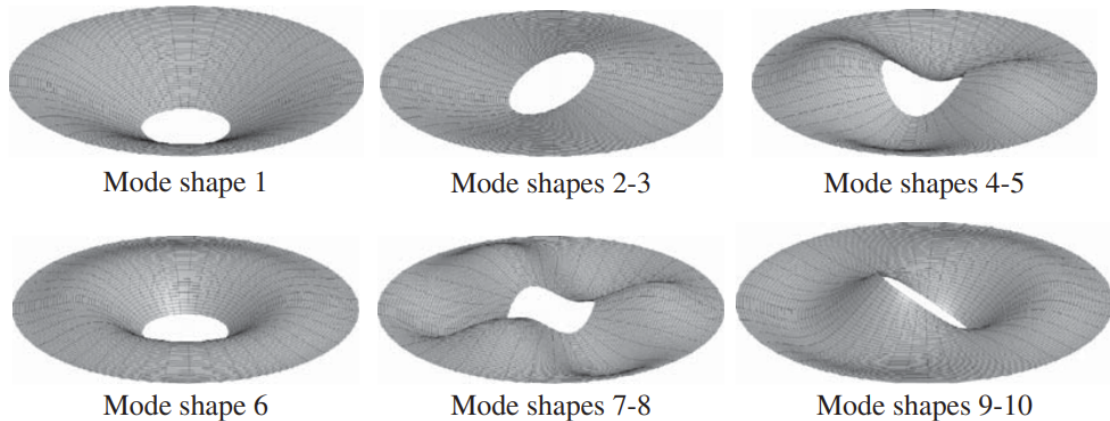


Figure 10 Mode shapes of annular plates with fixed boundary conditions on the outer edge and free boundary conditions on the inner edge<sup>37</sup> (Figure taken from; Tornabene et al.).

## 2.6 Effective mass

In the dynamics of resonators such as beams, cantilevers, or membranes only a portion of the resonator's total mass actively participates in its vibrational motion<sup>7</sup>. This amount of mass which participate in the vibrational motion is often called effective mass. The effective mass of resonators is determined not only by the physical mass of the material but also by the distribution of that mass in relation to the mode shape of vibration. This makes the effective mass a critical parameter in the design and application of NEMS<sup>7,38</sup>.

This effective mass can be determined by taking the total mass and multiplying it by the integral of a function that uses the normalized mode shape of resonance (Eq. 2.21

which will be discussed). For example, in the case of a doubly clamped beam vibrating in its fundamental mode, the effective mass is less than 73% of the total mass<sup>7</sup>.

For membrane nanoresonators, the effective mass is often much smaller than the physical mass of the material itself<sup>36</sup> (Table 2) due to the predominant role of surface effects over bulk material properties.

Mode Label ( <i>m, n</i> )	$m_{\text{eff},mn}/m$	
	EMI – Analytical	EMI – FEM
(0,1)	0.2695	0.2693
(1,1)	0.2396	0.2394
(2,1)	0.2437	0.2435
(0,2)	0.1158	0.1188
(3,1)	0.2357	0.2356
(1,2)	0.1330	0.1329
(4,1)	0.2254	0.2253
(2,2)	0.1556	0.1555
(0,3)	0.0737	0.0753
(5,1)	0.2152	0.2151

Table 2 Comparison of the effective mass to total mass ratio for a circular membrane across various resonance modes. For each mode, the ratio is determined using the Effective Mass Integral (EMI), calculated both analytically and via finite element analysis<sup>36</sup> (Table taken from; Hauer et al.).

In this thesis, determining the effective mass of membranes is essential, thus methodologies for calculating the effective mass for rectangular, circular, and annular membranes are included in here. These calculations are based on the specific mode shape under consideration, as the effective mass varies with the vibrational mode of the membrane.

The effective mass for the  $n^{\text{th}}$  mode of a resonator can be calculated by analyzing its potential energy. In this mode, every tiny volume element  $dV$  of the resonator possesses a potential energy  $dU$ <sup>36</sup>:



$$dU = \frac{1}{2} \rho(r) \omega_n^2 |a_n(t) r_n(x)|^2 dV \quad (2.17)$$

Therefore, the total potential energy will be like<sup>36</sup>:

$$U = \frac{1}{2} \omega_n^2 |a_n(t)|^2 \int dV \rho(r) |r_n(x)|^2 \quad (2.18)$$

The integral part is defined as the effective mass, so<sup>36</sup>:

$$U = \frac{1}{2} \omega_n^2 |a_n(t)|^2 m_{\text{eff},n} \quad (2.19)$$

$$m_{\text{eff},n} = \int dV \rho(r) |r_n(x)|^2 \quad (2.20)$$

Assuming that the material is isotropic, the mass density of the material is constant everywhere, we would obtain<sup>36</sup>:

$$m_{\text{eff},n} = \rho \int dV |r_n(x)|^2 \quad (2.21)$$

For rectangular membranes, the effective mass calculation involves integrating the mass distribution over the area influenced by the particular mode shape of vibration<sup>36</sup>.

$$m_{\text{eff},mn} = \frac{m}{L_x L_y} \int_0^{L_y} \int_0^{L_x} dx dy |\psi_{mn}(x, y)|^2 \quad (2.22)$$

Where  $m$  is the mass of the membrane,  $L_x$  and  $L_y$  are the dimensions of the rectangular membrane, and  $\psi_{mn}$  is the normalized mode shape we want to study.

For circular membranes the effective mass is calculated by considering the mode shapes in the radial and circumferential coordinates<sup>36</sup>:

$$m_{\text{eff},mn} = \frac{m}{\pi a^2} \int_0^{2\pi} d\varphi \int_0^a s ds |\psi_{mn}(s, \varphi)|^2 \quad (2.23)$$

In which,  $a$  is the radius of the circular membrane.

Annular membranes, which are circular membranes with a central hole, present a unique challenge due to the discontinuity introduced by the hole. The effective mass in this case is determined by the modified boundary conditions and the resultant mode shapes, which can differ from those of a full circular membrane:

$$m_{\text{eff},mn} = \frac{m}{\pi(a^2-b^2)} \int_0^{2\pi} d\varphi \int_b^a s ds |\psi_{mn}(s, \varphi)|^2 \quad (2.24)$$

In which,  $a$  is the outer radius and  $b$  is the inner radius of the annular membrane.

## 2.7 Coupled nanomechanical resonators

Systems of coupled nanomechanical resonators are typically composed of two or more nanoscale resonators, such as beams, membranes, or cantilevers, coupled together to form a system that exhibits collective vibrational modes. The interaction between the resonators can be direct, through physical connections<sup>39</sup>, or indirect, mediated by electromagnetic fields<sup>40</sup>, depending on the design and intended application of the system.

The dynamics of coupled nanomechanical resonators are governed by the principles of coupled harmonic oscillators. The coupling introduces new modes of vibration that are a combination of the individual resonators' modes, leading to a rich spectrum of mechanical behavior. This coupling can lead to a variety of interesting phenomena, such as enhanced sensitivity in measurements and mode splitting.

In the study of nanomechanical resonator systems, coupled harmonic oscillators provide a fascinating insight into the dynamics of interconnected structures<sup>41</sup>. A classic

example of such a system is a two-degree-of-freedom (2 DOF) model consisting of two masses connected by springs, with two more spring connecting each of the masses to fixed points, resulting in a 2 mass, 3 spring system (Figure 11).

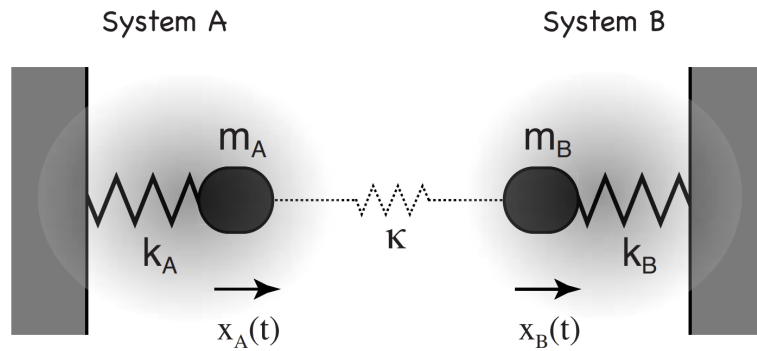


Figure 11 Schematic of 2-mass-3-spring 2DOF system. The central spring ( $\kappa$ ) links two one-degree-of-freedom (1 DOF) systems (System A and System B), each consisting of a mass ( $m_A$  and  $m_B$ ) and a spring ( $k_A$  and  $k_B$ ), to form a coupled two-degree-of-freedom (2 DOF) system of oscillators. This coupling facilitates the transfer of vibrational energy between the two systems, creating a coupled system<sup>41</sup> (Figure taken from; Novotny).

In the absence of the middle spring ( $k$ ), System A and System B would oscillate independently as two separate one-degree-of-freedom systems. However, with the introduction of the middle spring, they become coupled, leading to a synchronized oscillation. By applying Newton's second law to each mass and considering the forces applied by the springs, we can derive the equations of motion for this coupled system<sup>41</sup>:

$$m_A \ddot{x}_A + k_A x_A + \kappa(x_A - x_B) = 0 \quad (2.25)$$

$$m_B \ddot{x}_B + k_B x_B + \kappa(x_B - x_A) = 0 \quad (2.26)$$

Solving these coupled ordinary differential equations (ODEs) leads to the eigenfrequencies of the system<sup>41</sup>:

$$\omega_{\pm}^2 = \frac{1}{2} \left( \left( \frac{k_A + \kappa}{m_A} + \frac{k_B + \kappa}{m_B} \right) \pm \sqrt{\left( \frac{k_A + \kappa}{m_A} - \frac{k_B + \kappa}{m_B} \right)^2 + \frac{4\kappa^2}{m_A m_B}} \right) \quad (2.27)$$

In which  $\omega_{\pm}$  are the eigenfrequencies of the 2-DOF system. The stiffness of the middle spring, denoted by  $\kappa$ , determines the coupling strength within the coupled system<sup>41</sup>.

In this system of connected oscillators, altering the stiffness of one of the springs ( $k_A$  or  $k_B$ ) and plotting the eigenfrequencies versus this change, will reveal a phenomenon known as an avoided crossing in the graph (Figure 12). An avoided crossing signals strong coupling within the system. The difference in frequencies, often referred to as frequency splitting ( $\Gamma$ ), can be computed as follows<sup>41</sup>:

$$\Gamma = \frac{\kappa}{\sqrt[4]{(\kappa + k_A)(\kappa + k_B)m_A m_B}} \quad (2.28)$$

This relation shows that  $\Gamma$  will grow larger as the strength of the coupling increases.

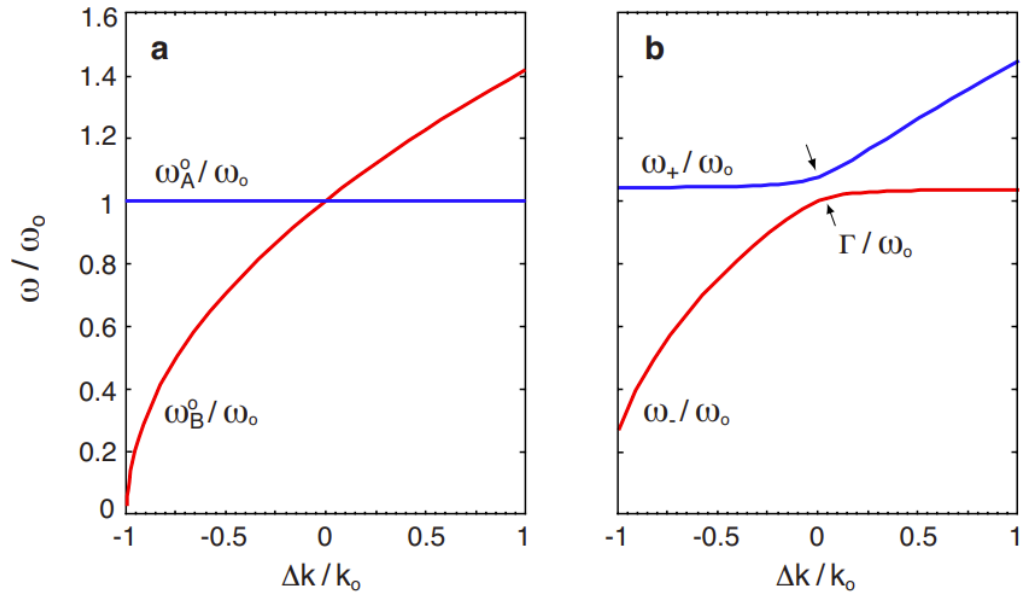


Figure 12 Assuming  $k_A = k_0$  and  $k_B = k_0 + \Delta k$ ; without coupling, the two curves intersect at  $\Delta k = 0$ . With coupling introduced, the curves no longer intersect but exhibit an avoided crossing, indicative of strong coupling<sup>41</sup> (Figure taken from; Novotny).

In nanoresonators, avoided crossing, also recognized as anti-crossing, indicates strong coupling between two vibrational modes. This effect can arise from several sources, including changes to the stiffness of the nanoresonator material, which can occur through external factors such as exposure to a laser beam. For example, in a system of two coupled nanoresonators, if one experiences a change in stiffness due to laser-induced heating, the resonance frequencies of the coupled system can shift, resulting in avoided crossing<sup>39</sup> (Figure 13).

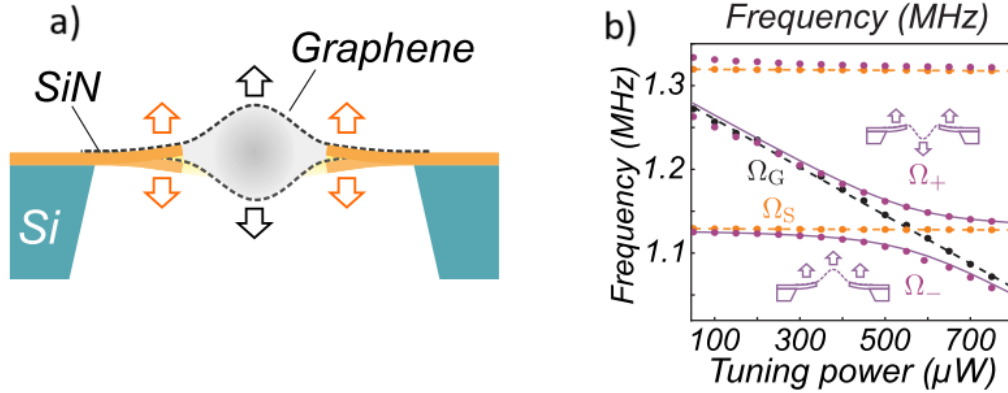


Figure 13 a) Schematic of coupled graphene and silicon nitride nanoresonators<sup>39</sup>. b) Hybridization between graphene and silicon nitride modes;  $\Omega_G$  is the uncoupled graphene mode,  $\Omega_S$  is the uncoupled silicon nitride mode, and  $\Omega_{\pm}$  are the hybridized mode<sup>39</sup> (Figures taken from; Schwarz et al.).

## 2.8 Vibrations of pressurized membrane

Atomically thin, pressurized membranes serve as highly sensitive components for pressure sensors. Understanding the vibrations of these pressurized membranes is crucial. In this section, I include derivations based on an energy approach proposed by Yousefi to estimate the fundamental natural frequency of a pressurized MoS<sub>2</sub> membrane<sup>42</sup>.

The energy method for determining the natural frequency of a system utilizes the Euler-Lagrange equation:

$$L \equiv T - V \quad (2.29)$$

Here, T represents the kinetic energy, and V denotes the potential energy of the system. By applying the derivative:

$$\frac{d}{dt} \left( \frac{\partial L}{\partial \dot{z}} \right) - \frac{\partial L}{\partial z} = 0 \quad (2.30)$$

and substituting L from Eq. 2.29 into it, we obtain:

$$\ddot{z} + \omega_n^2 z = 0 \quad (2.31)$$

where  $\omega_n$  represents the natural frequency of the system.

To determine the natural frequencies of a pressurized membrane, we start by assuming that the membrane, when in static equilibrium under applied pressure, has a maximum deflection denoted by  $\delta$ . This deflection can be derived from Hencky's solution<sup>43</sup>. The gas cavity's volume beneath the membrane under such conditions is given by<sup>42</sup>:

$$V_{b1} = C_1 \pi a^2 \delta \quad (2.32)$$

Where  $a$  represents the radius of the circular membrane, and  $C_1$  is a constant related to Poisson's ratio. For MoS<sub>2</sub>,  $C_1$  has been determined to be 0.522<sup>44</sup>. During vibration, the central deflection of the membrane is considered to be  $\delta + z$ . By considering the first mode of vibration, the volume of the gas cavity can be expressed as follows<sup>42</sup>:

$$V_{b2} = C_1 \pi a^2 (\delta + z) \quad (2.33)$$

The kinetic and potential energy of the system can be formulated as<sup>42</sup>:

$$T = \frac{1}{2} \alpha m \dot{z}^2 \quad (2.34)$$

$$U = U_2 - U_1 \quad (2.35)$$

where<sup>45</sup>:

$$\alpha = \frac{m_{eff}}{m} \quad (2.36)$$

$$U_2 = \frac{\Delta P_2 V_{b2}}{4} - P_0 V_0 \ln \left( 1 + \frac{V_{b2}}{V_0} \right) + P_{ext} V_{b2} \quad (2.37)$$

$$U_1 = \frac{\Delta P_1 V_{b1}}{4} - P_0 V_0 \ln \left( 1 + \frac{V_{b1}}{V_0} \right) + P_{ext} V_{b1} \quad (2.38)$$

In these equations,  $P_{ext}$  represents the external pressure on the membrane, and the pressure differences  $\Delta P_{1,2}$  could be calculated from:

$$\Delta P_2 = \frac{KE_{2d}(\delta+z)^3}{a^4} \quad (2.39)$$

$$\Delta P_1 = \frac{KE_{2d}\delta^3}{a^4} \quad (2.40)$$

Here,  $K$  is a constant related only to the Poisson's ratio. For  $\text{MoS}_2$ ,  $K$  is identified as 3.54<sup>44</sup>. Substituting  $T$  and  $U$  into the energy equation (2.30) yields<sup>42</sup>:

$$(\alpha \rho_A \pi a^2) \ddot{z} + \left( \frac{3C_1 K \pi E_{2d} \delta^2}{a^2} + \frac{C_1^2 P_{int} \pi a^2}{h + C_1 \delta} \right) z = 0 \quad (2.41)$$

Finally, the calculation results in<sup>42</sup>:

$$f_{breath.+Helmholtz} = \frac{1}{2\pi} \sqrt{\frac{3C_1}{\alpha} \cdot \frac{P_{int}-P_{ext}}{\delta \rho_A} + \frac{C_1^2}{\alpha} \cdot \frac{P_{int}}{\rho_A} \cdot \frac{1}{h+C_1\delta}} \quad (2.42)$$



## 2.9 Derivations of finite element for vibrations

The resonance frequency of micro- or nanoscale resonators is achievable through analytical methods grounded in continuum mechanics or through finite element method (FEM) simulations. Analytical approaches, by simplifying the structures into ideal forms, might miss specific details of the actual resonator. However, they offer significant insights into how the design and material choices affect the vibrational modes<sup>33</sup>. Consequently, FEM becomes helpful for capturing these complicated details, providing a comprehensive understanding that bridges the gap between theoretical models and real-world applications.

### 2.9.1 FEM for eigenfrequencies

Finite element formulations for natural frequencies involves a systematic process that starts from the basic principles of mechanics and applies the finite element method (FEM) to solve the relevant differential equations. The general approach includes discretizing the system into finite elements, formulating the element equations based on the principle of virtual work or energy methods, assembling the global system equations, and then solving the eigenvalue problem to find the natural frequencies<sup>46</sup>.

The derivation of the finite element method (FEM) for calculating eigenfrequencies in mechanical systems involves transitioning time-dependent problems into a series of ordinary differential equations. These equations typically represent a characteristic form that integrates mass (M), damping (C), stiffness (K) matrices, and an external force vector (f), structured as<sup>46</sup>:

$$M\ddot{u} + C\dot{u} + Ku + f = 0 \quad (2.43)$$

In the absence of damping and external forces, this dynamic equation simplifies to:

$$M\ddot{u} + Ku = 0 \quad (2.44)$$

This equation highlights the system's natural vibratory state. The solution to this simplified equation represents harmonic motion, where:

$$u = \bar{u} \exp(i\omega t) \quad (2.45)$$

With  $\omega$  denoting the system's natural frequencies. This leads us to the eigenvalue problem:

$$(-\omega^2 M + K)\bar{u} = 0 \quad (2.46)$$

Zero solutions necessitating that:

$$|-\omega^2 M + K| = 0 \quad (2.47)$$

Solving this determinant equation yields the eigenfrequencies of the system.

Key elements in this process include the mass matrix (M), which represents the system's inertia, and the stiffness matrix (K), which characterizes the system's rigidity. The damping matrix (C), though omitted in the simplified eigenfrequency calculation, accounts for energy dissipation within the system. These matrices are assembled from their elemental counterparts,  $M_e$  and  $K_e$ , calculated over the discretized model of the structure<sup>46</sup>.

Elemental matrices,  $C_e$ ,  $M_e$ , and  $K_e$ , are derived from the integration over each element, reflecting the distribution of mass and damping properties within that element. The assembled system matrices, K, M and C, combine these elemental contributions to

represent the entire system's dynamic characteristics.

### 2.9.2 FEM for coupled vibrations

In mechanically coupled systems, where physics are linked via an interface, the system is often divided into components that are joined along this interface. Different components may employ varying sizes and methods of discretization. In such problems, coupling takes place at the domain interface, determined by the boundary conditions applied there<sup>46</sup>.

The FEM formulation for a system of coupled oscillators can be captured by a system of ordinary differential equations, typically represented as Eq. (2.29). This equation can be divided into components for each substructure, leading to a partitioned form<sup>46</sup>:

$$\begin{bmatrix} M_{11} & M_{12} \\ M_{21} & M_{22} \end{bmatrix} \begin{Bmatrix} \ddot{u}_1 \\ \ddot{u}_2 \end{Bmatrix} + \begin{bmatrix} C_{11} & C_{12} \\ C_{21} & C_{22} \end{bmatrix} \begin{Bmatrix} \dot{u}_1 \\ \dot{u}_2 \end{Bmatrix} + \begin{bmatrix} K_{11} & K_{12} \\ K_{21} & K_{22} \end{bmatrix} \begin{Bmatrix} u_1 \\ u_2 \end{Bmatrix} + \begin{Bmatrix} f_1 \\ f_2 \end{Bmatrix} = \begin{pmatrix} 0 \\ 0 \end{pmatrix} \quad (2.48)$$

## CHAPTER 3. MODELING OF COUPLED NANORESONATORS

### 3.1 Introduction

This chapter focuses on Finite Element (FE) simulations of the coupled silicon nitride ( $\text{SiN}_x$ ) drumhead and molybdenum disulfide ( $\text{MoS}_2$ ) membrane systems. These simulations are crucial for understanding the complex mechanical behaviors and vibrational characteristics of nanomechanical systems. Despite Yousefi's pioneering experimental investigations into these resonators, a computational exploration of their coupled dynamics remains uncharted<sup>42</sup>. This gap signifies the necessity of FE simulations to complement experimental findings and offer predictive insights into the behavior of these advanced materials when integrated into a system.

### 3.2 FE simulations of $\text{SiN}_x$ drumhead

#### 3.2.1 *Simulation setup and model configuration*

This simulation was conducted within the Structural Mechanics module, specifically employing the Solid Mechanics physics interface. The geometric model represents an annular drumhead with defined inner and outer radii, reflecting the physical dimensions encountered in microfabricated device in our lab. The material properties assigned to the model are based on those of silicon nitride, with considerations for density, Young's modulus, and Poisson's ratio, ensuring that the simulations mirror the real-world behavior of the material under mechanical stress.

<b>Parameter</b>	<b>Value</b>
Outer Diameter	17 $\mu\text{m}$
Inner Diameter	4 $\mu\text{m}$
Thickness	100 nm
Initial Tension	200 MPa

Table 3 Model configuration of annular-shaped silicon nitride drumhead.

The boundary conditions are set to match the fixed support around the outer perimeter of the drumhead, while the inner edge is left free to vibrate, mimicking the conditions of the real annular membrane under tension.

<b>Properties</b>	<b>Value</b>
Density	3100 kg/m <sup>3</sup>
Young's Modulus	250 GPa
Poisson's Ratio	0.23

Table 4 Mechanical properties of silicon nitride.

### 3.2.2 *Simulation results*

In this part of the chapter, we present the results from an eigenfrequency study in COMSOL for the annular-shaped silicon nitride drumhead. The results include the mode shapes, natural frequencies, and effective masses for each vibrational mode, detailed in a comprehensive table. The table provides a comparative view of how natural frequencies and effective masses vary across different modes.

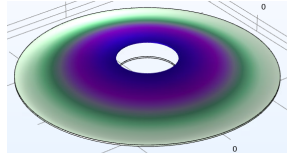
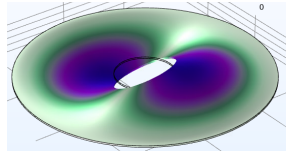
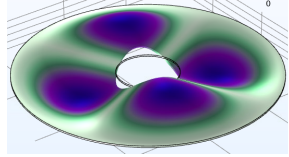
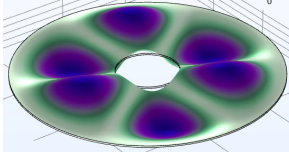
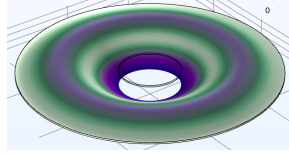
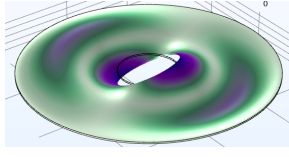
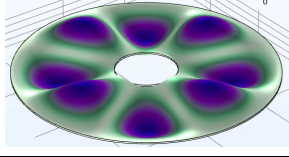
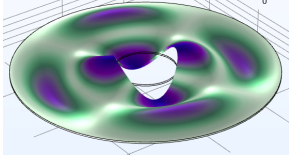
Mode Index (m,n)	Mode Shape	Frequency (MHz)	$m_{\text{eff}}$ (kg)	$m_{\text{eff}}/m$
(0,1)		15.26	$1.576 \times 10^{-14}$	0.2370
(1,1)		21.10	$1.221 \times 10^{-14}$	0.1837
(2,1)		31.56	$1.484 \times 10^{-14}$	0.2233
(3,1)		43.01	$1.475 \times 10^{-14}$	0.2219
(0,2)		43.51	$8.523 \times 10^{-15}$	0.1282
(1,2)		48.57	$4.710 \times 10^{-15}$	0.0709
(4,1)		55.23	$1.422 \times 10^{-14}$	0.2140
(2,2)		61.20	$7.529 \times 10^{-15}$	0.1133

Table 5 COMSOL analysis for eight distinct vibrational modes for the annular-shaped silicon nitride drumhead.

To calculate the effective mass for each mode, I used a method involving the surface integral in COMSOL over the drumhead's deformed shape after vibration. Based on Eq. 2.24 for calculating the effective mass, first we should calculate the normalized deformation,  $\psi(r,\varphi)$ , which is the deformation in each point divided by the maximum deformation of the structure. Then I calculated the integral of  $\psi$  over the drumhead surface. By dividing the result by  $\pi(a^2 - b^2)$ , the ratio of effective mass to the real mass of the drumhead is reached. We will need the results of the effective mass of each mode of vibration of silicon nitride drumhead in future part of this chapter to calculate the coupling constant between different modes of silicon nitride and MoS<sub>2</sub>.

### **3.3 FE simulations of MoS<sub>2</sub> membrane**

This section presents the outcomes of a finite element analysis performed on a circular MoS<sub>2</sub> membrane. The simulation utilized the Membrane Physics interface within the Structural Mechanics module of COMSOL Multiphysics, designed for examining the mechanical behavior of thin membrane structures.

#### *3.3.1 Simulation setup and model configuration*

The simulation on a circular MoS<sub>2</sub> membrane is designed to match the exact dimensions in microfabricated devices from our lab. We input mechanical properties like density, Young's modulus, and Poisson's ratio according to established MoS<sub>2</sub> properties.

Parameter	Value
Diameter	4 $\mu\text{m}$
Thickness	6.5 $\text{\AA}$
Pretension	0.062 N/m

Table 6 Model configuration of circular MoS<sub>2</sub> membrane.

Boundary conditions are defined to emulate real-world scenarios: the membrane outside edge was fixed to simulate a clamped edge, whereas the central area was allowed to vibrate freely.

Properties	Value
Density	5060 kg/m <sup>3</sup>
2D Young's Modulus	128 N/m
Poisson's Ratio	0.29

Table 7 Mechanical properties of MoS<sub>2</sub>.

### 3.3.2 Simulation results

The results section showcases findings from the eigenfrequency analysis, highlighting mode shapes, natural frequencies, and effective masses for various vibrational modes of the MoS<sub>2</sub> membrane. The following table contains the natural frequencies and effective masses across different modes.



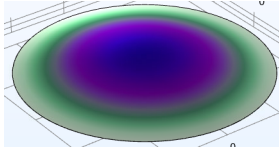
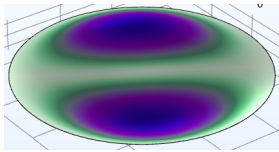
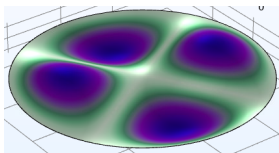
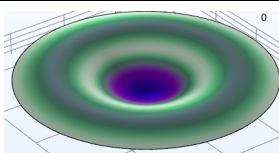
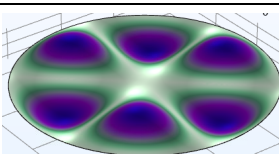
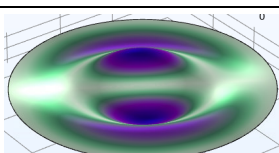
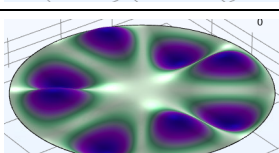
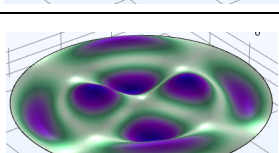
Mode Index (m,n)	Mode Shape	Frequency (MHz)	$m_{\text{eff}}$ (kg)	$m_{\text{eff}}/m$
(0,1)		26.28	$1.114 \times 10^{-17}$	0.2695
(1,1)		41.87	$9.902 \times 10^{-18}$	0.2396
(2,1)		56.11	$1.008 \times 10^{-17}$	0.2438
(0,2)		60.31	$4.786 \times 10^{-18}$	0.1158
(3,1)		69.71	$9.744 \times 10^{-18}$	0.2357
(1,2)		76.65	$5.499 \times 10^{-18}$	0.1330
(4,1)		82.91	$9.321 \times 10^{-18}$	0.2255
(2,2)		91.97	$6.430 \times 10^{-18}$	0.1556

Table 8 COMSOL analysis for eight distinct vibrational modes for the circular MoS<sub>2</sub> membrane.

The effective mass, similar to silicon nitride, is calculated by performing a surface integral over the membrane's deformed shape post-vibration. This process involved first determining the normalized deformation,  $\psi(r,\phi)$  by dividing the deformation at each point by the structure's maximum deformation. Subsequently, an integral of  $\psi$  across the membrane surface was executed. The final step involved dividing the integral's outcome by  $\pi a^2$  to find the ratio of the effective mass to the actual mass of the membrane.

Similar to silicon nitride, these effective mass outcomes are critical for subsequent analyses in this chapter such as evaluating the coupling constant between various vibrational modes of the MoS<sub>2</sub> membrane and silicon nitride.

### **3.4 FE simulations of coupled SiN<sub>x</sub> drumhead and MoS<sub>2</sub> membrane**

#### *3.4.1 Motivation*

The motivation behind conducting COMSOL simulations of the coupled MoS<sub>2</sub> and silicon nitride resonators is based on a gap identified in the existing body of research. While Yousefi's experimental work laid a foundational understanding of these resonators' behavior, it did not extend to include simulations of the coupled systems. This gap represents a significant opportunity for further exploration, particularly in understanding the interactions and vibrational dynamics of the coupled MoS<sub>2</sub> and silicon nitride resonators.

Simulations offer a powerful tool for predicting and visualizing the complex behaviors of such coupled systems under various conditions without the limitations and practical challenges of experimental setups. This computational approach allows for a

comprehensive analysis of the effects of coupling on the vibrational characteristics of the system, providing insights that are valuable for both theoretical understanding and practical applications.

### *3.4.2 Simulation and analysis*

Following the independent simulations of the silicon nitride drumhead and the MoS<sub>2</sub> membrane, a comprehensive simulation has been done to explore the dynamics of a coupled system composed of the drumhead and the membrane. This analysis, facilitated by the Multiphysics capabilities of COMSOL, applied specific coupling boundary conditions at the contact interface of the drumhead and membrane.

For the simulation of coupled nanoresonators, the 3D interface of COMSOL is utilized. The annular-shaped silicon nitride geometry is created using SOLIDWORKS, after which it is imported into COMSOL. To define the geometry of the membrane, a work plane is established parallel to and coinciding with the upper surface of the silicon nitride structure.

The materials, silicon nitride and MoS<sub>2</sub>, are specified according to the mechanical properties listed in Tables 3 and 6, and are assigned to their respective geometries. Silicon nitride utilizes solid mechanics physics because the silicon nitride drumhead is treated not as a membrane but as a solid structure. Conversely, MoS<sub>2</sub> is modeled using membrane physics.

Within the membrane physics settings, the thickness of the MoS<sub>2</sub> layer is set at  $6.5 \times 10^{-10}$  meters, specified under the "thickness and offset" node, with the positioning option set to "bottom surface on boundary." The simulation's boundary conditions include

a fixed constraint along the outer edge of the silicon nitride annular drumhead.

Coupling is achieved by establishing a "thin-solid connection" under the Multiphysics node, employing a "shared boundary" connection type at the contact surface. This setup simulates the drumhead and membrane as being fully adhered at their interface.

To determine the natural frequencies of the coupled system, tetrahedral meshing is used for the problem's discretization and an eigenfrequency study using geometric nonlinearity in settings is used.

The results, detailed in Table 9, show the presence of vibrational frequencies of both the silicon nitride and MoS<sub>2</sub> components within the hybrid modes.

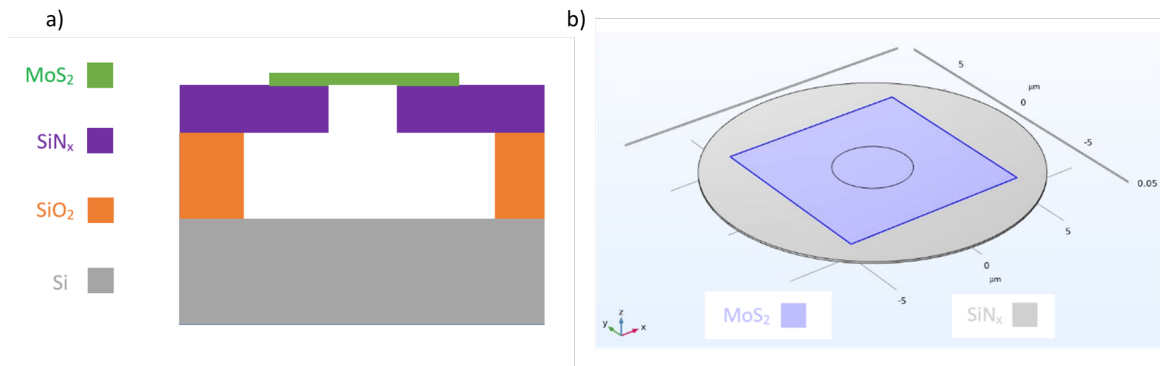


Figure 14 a) Schematic of the experimental geometry (side view). b) Simulation geometry in COMSOL.

	SiN <sub>x</sub> Coupled Mode Shape	MoS <sub>2</sub> Coupled Mode Shape	Frequency (MHz)
Larger amplitude of deformation in vibration  Smaller amplitude of deformation in vibration mode			15.18
			21.05
			26.28
			31.5
			41.80
			42.97
			43.47
			48.61

Table 9 COMSOL analysis for eight distinct vibrational modes for the coupled MoS<sub>2</sub> membrane and silicon nitride drumhead. The setup parameters for both the membrane and drumhead are same as those described in sections 3.2 and 3.3, with the modification that the membrane now has a 10 $\mu\text{m}$   $\times$  10 $\mu\text{m}$  square shape.

Building on this foundation, the simulation further mimicked a heating process similar to an experimental procedure conducted by Fartash in our laboratory. This process is targeting the center of the MoS<sub>2</sub> membrane with a laser beam. The heat generated by the laser leads to a gradual release of the membrane's initial tension, in that way altering its natural frequency.

To achieve this objective, a parametric sweep is set up within the study node of the previously described model, adjusting the initial tension within the membrane from 0.062 N/m to 0.004 N/m to match the experimentally measured frequency changes. The eigenfrequencies calculated in COMSOL are exported to an Excel file, which is then imported into MATLAB. To visualize the impact of varying initial tension on the natural frequencies of the coupled system, a plot showing the relationship between the natural frequencies of the entire system and the tension in the MoS<sub>2</sub> membrane is generated using MATLAB. This plot is presented in Figure 15.

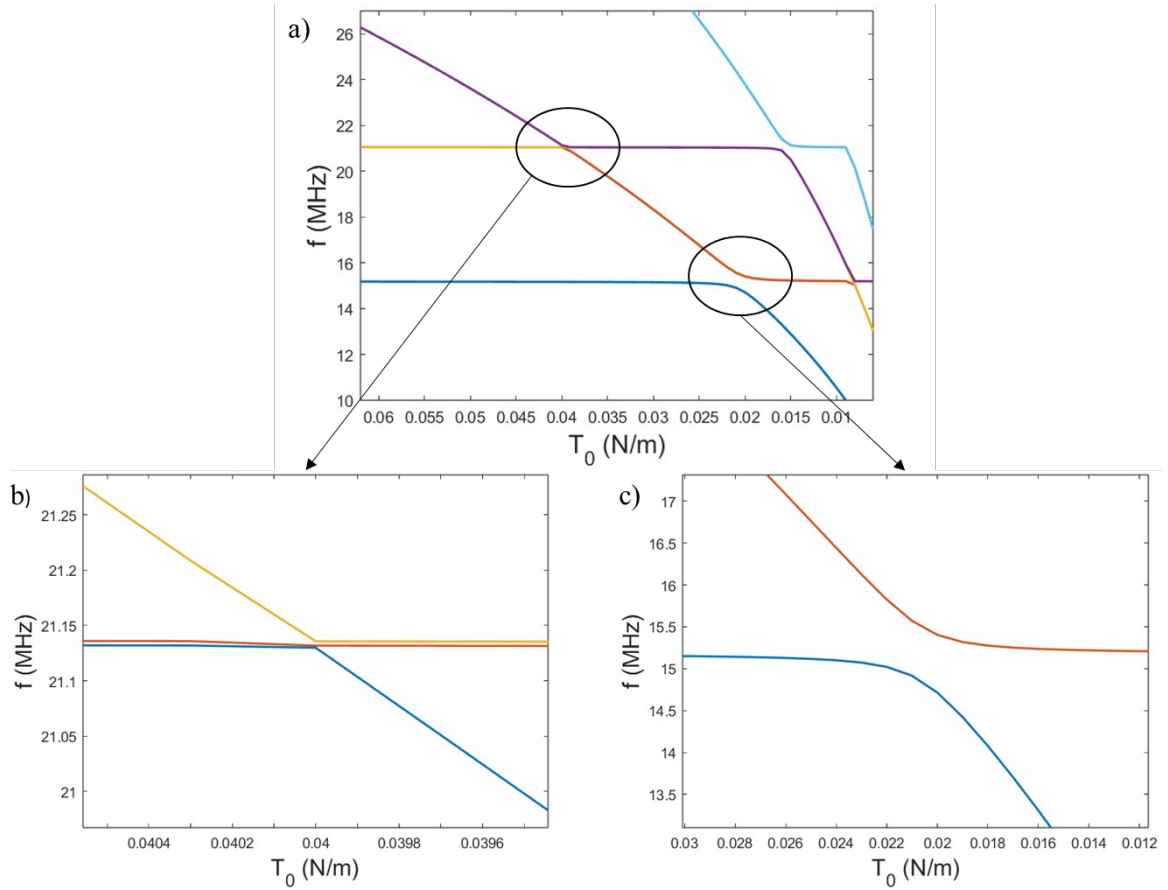


Figure 15 a) Natural frequencies of the coupled system consisted of SiNx drumhead and MoS<sub>2</sub> membrane plotted versus membrane tension; coupling between modes of MoS<sub>2</sub> and nitride sharing the same mode indices is stronger than coupling between modes with different indices. Each color represents a distinct mode of coupled system. b) Close-up view of the interaction between the first mode of MoS<sub>2</sub> and the second mode of nitride, showing weak coupling. c) Close-up view of the avoided crossing between the first mode of MoS<sub>2</sub> and the first mode of nitride, highlighting strong coupling.

Figure 15 showcases an interesting aspect of the coupled system's behavior. The horizontal lines within the figure denote the frequencies of the silicon nitride, serving as a reference for the system's behavior in the absence of tension changes. In contrast, the sharply inclined curves represent the MoS<sub>2</sub> frequencies, which are altering due to changes in MoS<sub>2</sub> tension. Although the decrease in tension might be expected to cause these MoS<sub>2</sub> frequency curves to intersect with the silicon nitride's frequencies, we observe a

phenomenon known as avoided crossing. Instead of intersecting, the curves distant from each other, avoiding direct crossing. This behavior is a clear indicator of strong coupling between the modes under investigation, suggesting a significant interactive influence between the silicon nitride and MoS<sub>2</sub> components of the system<sup>41</sup>.

To quantify this interaction, the following section of this chapter is dedicated to introducing a theoretical model capable of calculating the coupling constant. This model aims to provide a quantitative measure of the coupling strength observed in different instances of avoided crossing between the diverse modes of the silicon nitride and MoS<sub>2</sub> components.

### **3.5 Derivation of method for calculating coupling constant**

#### *3.5.1 Motivation*

Determining the coupling constant in nanomechanical resonator systems continues to be a key area of research, as evidenced by the work presented in Fartash's dissertation<sup>42</sup>. While his work presents a pioneering attempt to calculate the coupling constant, the estimations offered therein have room for improvement. This gap underscores the need for a refined approach to accurately measure this parameter, which is essential for understanding the dynamics of coupled nanomechanical systems.

The study of coupled harmonic oscillators has significantly advanced our comprehension of the complex interactions within nanomechanical resonator systems. A fundamental model used to explore these dynamics is the two-degree-of-freedom (2 DOF) system, composed of two masses linked by springs, with additional springs connecting



each mass to fixed points. This configuration, resembling a 2-mass-3-spring system (Figure 16), highlights the middle spring's stiffness as the coupling constant<sup>41</sup>.

Further exploration in the literature reveals two notable studies. The first paper investigated estimating the coupling constant between different modes of a beam nanomechanical resonator through curve fitting<sup>47</sup>. Similarly, the second paper applies curve fitting to estimate the coupling constant between different modes of MoS<sub>2</sub><sup>48</sup>. Both studies contribute valuable methodologies and insights, yet they focus on the coupling between different modes of a single material.

Building on this foundation, my approach aims to bridge these methodologies by applying curve fitting to a dual nanomechanical resonator system, including both MoS<sub>2</sub> and SiN<sub>x</sub>. This strategy involves conceptualizing the system as a 2-mass-3-spring harmonic oscillator (Figure 16), with the primary objective of determining the stiffness of the connecting spring, the coupling constant.

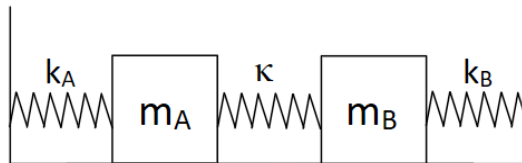


Figure 16 Schematic of a two-mass-three-spring 2 DOF system.

### 3.5.2 Model derivation

In this derivation, I begin by calculating the natural frequencies of the two-degree-of-freedom (2DOF) system, which consists of two masses and three springs:

$$m_A \ddot{x}_A + k_A x_A + \kappa(x_A - x_B) = 0 \quad (3.1)$$

$$m_B \ddot{x}_B + k_B x_B + \kappa(x_B - x_A) = 0 \quad (3.2)$$

$$f_{\pm}^2 = \frac{1}{2} \left( \left( \frac{k_A + \kappa}{4\pi^2 m_A} + \frac{k_B + \kappa}{4\pi^2 m_B} \right) \pm \sqrt{\left( \frac{k_A + \kappa}{4\pi^2 m_A} - \frac{k_B + \kappa}{4\pi^2 m_B} \right)^2 + \frac{4\kappa^2}{4\pi^2 m_A m_B}} \right) \quad (3.3)$$

Here,  $m_A$  and  $m_B$  represent the masses, while  $k_A$ ,  $k_B$ , and  $\kappa$  denote the stiffnesses of the springs. In our model of the MoS<sub>2</sub> membrane and SiN<sub>x</sub> drumhead,  $m_A$  corresponds to the effective mass of the silicon nitride for the specific mode being analyzed, and  $m_B$  corresponds to the effective mass of the MoS<sub>2</sub> for the mode under consideration. During the heating process, it's assumed that the stiffnesses of the MoS<sub>2</sub> and silicon nitride, denoted as  $k_A$  and  $k_B$ , change linearly from their initial values (prior to heating) in response to a variable  $Z$ :

$$k_1 = k_{10} - \alpha_1 Z \quad (3.4)$$

$$k_2 = k_{20} - \alpha_2 Z \quad (3.5)$$

Here,  $k_{10}$  and  $k_{20}$  are the stiffness initial values for the silicon nitride and MoS<sub>2</sub>, respectively. The corresponding formulations within the 2-mass-3-spring model, incorporating these initial stiffnesses, are presented as follows:

$$\frac{k_A}{4\pi^2} = \frac{\omega_A^2}{4\pi^2} - \frac{\alpha_A}{4\pi^2} (Z + \beta) \quad (3.6)$$

$$\frac{k_B}{4\pi^2} = \frac{\omega_B^2}{4\pi^2} - \frac{\alpha_B}{4\pi^2} (Z + \beta) \quad (3.7)$$

Here,  $\omega_A$  and  $\omega_B$  represent the natural frequencies of the silicon nitride and MoS<sub>2</sub> for the specific modes being examined, respectively, while  $m_A$  and  $m_B$  denote the effective masses of the silicon nitride and MoS<sub>2</sub> for these modes. The initial stiffness values prior to

heating are determined by dividing the square of the natural frequency for each mode by the corresponding effective mass of the silicon nitride and MoS<sub>2</sub>.

The subsequent step involves substituting these equations (3.6 and 3.7) into equation 3.3, resulting in two equations (for the '+' and '-' scenarios) that describe the frequency curves as functions of  $Z$ . To determine the coupling constant, we need to simultaneously match the two curves representing the avoided crossing (derived from simulation data points) with the two equations obtained after incorporating  $k_A$  and  $k_B$  into the natural frequency equations of the 2-mass-3-spring system. For this purpose, I utilized the “lsqcurvefit” function in MATLAB, capable of fitting two sets of data points simultaneously into two curves that share common variables.

### 3.5.3 *Coupling constant for SiNx and MoS<sub>2</sub> modes*

Employing the proposed model to compute the coupling constant in section 3.5.2, I determined the constants between different vibrational modes of silicon nitride and MoS<sub>2</sub>, leveraging the eigenfrequency analysis results from COMSOL.

Utilizing the frequency versus tension data illustrated in Figure 15c for the observed avoided crossing between the first mode of MoS<sub>2</sub> and the first mode of silicon nitride, I determined the coupling constant for these modes using MATLAB. I extracted the values for natural frequencies and effective masses of silicon nitride and MoS<sub>2</sub> from Tables 5 and 8, applying them as  $\omega_A$  (frequency of silicon nitride),  $m_A$  (effective mass of silicon nitride),

$\omega_B$  (frequency of MoS<sub>2</sub>) and  $m_B$  (effective mass of MoS<sub>2</sub>) in equations 3.6 and 3.7. Subsequently, by inserting  $k_A$  and  $k_B$  into equation 3.3, we obtain expressions for the coupled system's eigenfrequencies as functions of the variable “Z” and the unknown parameters “ $\alpha_A$ ,” “ $\alpha_B$ ,” “ $\beta$ ,” and “ $\kappa$ ”.

$$f_+^2 = f_1\left(Z, \frac{\alpha_A}{4\pi^2}, \frac{\alpha_B}{4\pi^2}, \beta, \frac{\kappa}{4\pi^2}\right) \quad (3.8)$$

$$f_-^2 = f_2\left(Z, \frac{\alpha_A}{4\pi^2}, \frac{\alpha_B}{4\pi^2}, \beta, \frac{\kappa}{4\pi^2}\right) \quad (3.9)$$

Through the simultaneous curve fitting of the avoided crossing's upper and lower branches into equations 3.8 and 3.9 using MATLAB's “lsqcurvefit” function, I calculated the unknown parameters, including the coupling constant “ $\kappa$ ”.

Figure 17 displays the avoided crossing observed between the first vibrational mode of silicon nitride and the first mode of MoS<sub>2</sub>. The data points in the figure are from the COMSOL simulation, while the continuous curves are generated from fitting the data point to the 2-mass-3-spring system. In this scenario, the coupling constant is calculated as 0.0042 N/m.

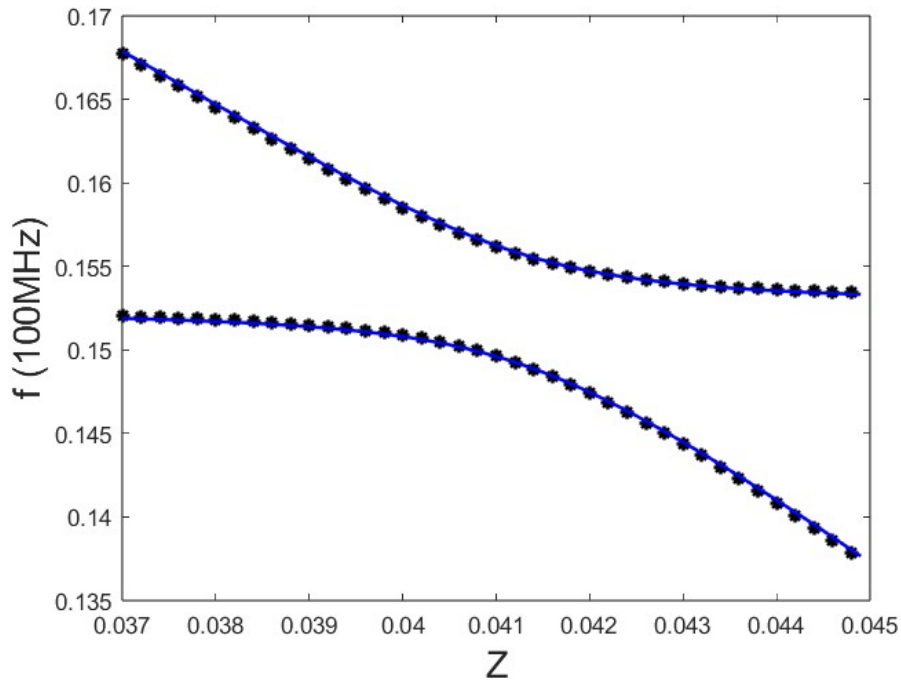


Figure 17 Curve fitted to the natural frequency data points from COMSOL simulations. The stars represent the data points, and the continuous curve illustrates the fit to these points. Here,  $Z = T_0 - T$ , where  $T_0$  is the initial tension in the membrane, and  $T$  is the tension at the specific frequency being analyzed. The coupling constant determined is 0.0042 N/m, with the error function (resnorm) achieving a value of  $2.2 \times 10^{-6}$ .

During these calculations, starting with certain initial guesses frequently led to imperfect curve fitting, indicated visually as well as by significant error values. To solve this problem, I used the "Multistart" optimization strategy. This method aims to identify the global minimum error rather than just a local minimum, enhancing the quality and precision of the fitting outcomes.

		$\frac{\kappa}{4\pi^2}$	
		<b>MoS<sub>2</sub> Modes</b>	
		<b>First</b>	<b>Second</b>
<b>SiN<sub>x</sub> Modes</b>	<b>First</b>	0.0042 N/m	0.0000 N/m
	<b>Second</b>	0.0004 N/m	0.0041 N/m

Table 10 Values for coupling constant over  $4\pi^2$  calculated through the model proposed.

Table 10 includes the coupling constants between the first two modes of MoS<sub>2</sub> and the first two modes of silicon nitride. As anticipated, the coupling strength of similar modes is significantly greater than that of dissimilar modes.

Although the simulation results for the coupled vibration match well with Yousefi's experimental findings, the calculated coupling constants differ from Yousefi's results. For instance, when examining the frequency versus tension graph derived from simulations, particularly focusing on the mode splitting between the first and second modes of MoS<sub>2</sub> and the second mode of silicon nitride, alongside Yousefi's experimental graph of frequencies versus laser power, highlighting the same modes in Figure 18, it's evident in both simulations and experiments that the mode splitting between the second mode of MoS<sub>2</sub> and the second mode of silicon nitride is more pronounced than the splitting between the first mode of MoS<sub>2</sub> and the second mode of silicon nitride. Given that larger mode splitting suggests stronger coupling and a larger coupling constant<sup>41</sup>, we expect higher coupling constants between the second modes of MoS<sub>2</sub> and silicon nitride compared to the

coupling between the first mode of MoS<sub>2</sub> and the second mode of silicon nitride. I calculated these constants as 0.0041 N/m and 0.0004 N/m, respectively. However, Yousefi's experimental results contradict the model, reporting a smaller coupling constant for the second mode of MoS<sub>2</sub> and the second mode of silicon nitride than for the first mode of MoS<sub>2</sub> and the second mode of silicon nitride. Further work is necessary to understand this discrepancy.

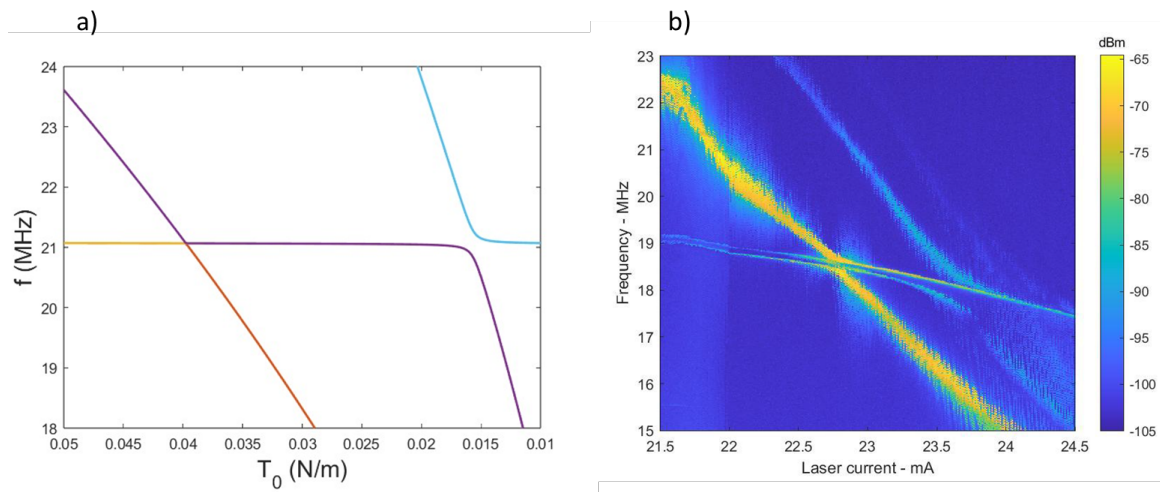


Figure 18 a) Simulated natural frequencies of the coupled system versus tension in the MoS<sub>2</sub>. b) Experimentally measured natural frequencies versus laser power from Yousefi's work (Figure b taken from; Yousefi). Both figures highlight more significant mode splitting, indicative of stronger coupling, between the second mode of MoS<sub>2</sub> and the second mode of silicon nitride compared to the mode splitting between the first mode of MoS<sub>2</sub> and the second mode of silicon nitride.

### 3.6 Conclusion

In this chapter, Finite Element simulations of the coupled SiN<sub>x</sub> drumhead and MoS<sub>2</sub> membrane systems have advanced our understanding of their vibrational dynamics. By calculating the coupling constants, we have identified that identical modes couple more strongly than dissimilar ones, offering insights into optimizing nanomechanical system

designs. My simulations and the calculation of coupling constants between various modes of MoS<sub>2</sub> and silicon nitride provide valuable insights into Yousefi's experimental observations. These findings not only bridge existing research gaps but also set the stage for future innovations in nanodevice development.



## CHAPTER 4. MODELING OF PRESSURIZED MEMBRANE

### 4.1 Introduction

Applying pressure to two-dimensional materials that are clamped and suspended is a straightforward approach to subject atomic membranes to significant stress. These pressurized membranes, due to their high sensitivity, are excellent candidates for pressure sensors. The study of vibrations in membranes pressurized by gas has been extensive. Henchy developed a model for the deformation of circular clamped membranes under pressure, while Fichter offered corrections to Henchy's analysis for circular pressurized membranes<sup>43</sup>. Dolleman et al. explored the squeeze-film effect on single-layer pressurized graphene membranes<sup>3</sup>. Additionally, Bodetti et al. and Lloyd et al. investigated the adhesion energy between pressurized atomic membranes and substrates<sup>45,49</sup>. Sarafraz et al. presented a model to estimate the natural frequencies of pressurized membranes, considering not only the tension created by gas pressure but also changes in the membrane's shape<sup>50</sup>. Moreover, Yousefi's Ph.D. dissertation proposed a model for calculating the fundamental natural frequency of a pressurized membrane in conjunction with the Helmholtz resonance of the gas below<sup>42</sup>. In this chapter, we incorporate Finite Element simulations of a MoS<sub>2</sub> membrane pressurized with Argon gas to further this line of inquiry.

Yousefi fabricated a circular MoS<sub>2</sub> membrane over a cylindrical argon gas cavity. Figure 19 schematically illustrates the deformation of the membrane in response to changes in external pressure. The pressure within the cavity remains relatively constant due to the impermeability of the MoS<sub>2</sub> membrane.

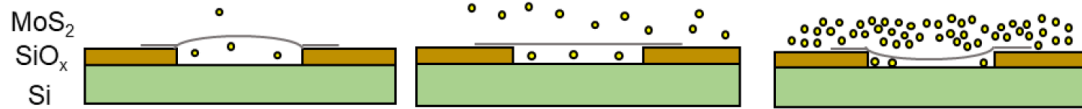


Figure 19 Schematic of deformation of membrane due to changes in external pressure, assuming that the internal pressure is constant<sup>42</sup>. (Figure taken from; Yousefi)

In the scenario where a MoS<sub>2</sub> membrane is pressurized over a gas cavity, three primary mechanisms influence the natural frequencies of the membrane. The initial mechanism involves tension induced by the membrane's deformation. As the membrane deforms, tension increases, which consequently raises the vibration frequencies. The second mechanism is the action of the gas within the cavity, functioning similarly to a spring. When the membrane vibrates upwards, the cavity's pressure decreases, exerting a force that pushes the membrane back towards its equilibrium position, and the reverse occurs when the membrane vibrates downwards. This behavior justifies modeling the gas as a spring for simulation purposes. The third mechanism is the interaction between the vibrational resonance of the membrane and the acoustic resonance of the gas, which also affects the tuning of the membrane's frequencies.

Figure 20 illustrates three distinct mass-spring systems, each representing the effects of the mechanisms influencing the vibrations of the membrane. These systems provide a simplified visual explanation of how each mechanism impacts the membrane's dynamic behavior.

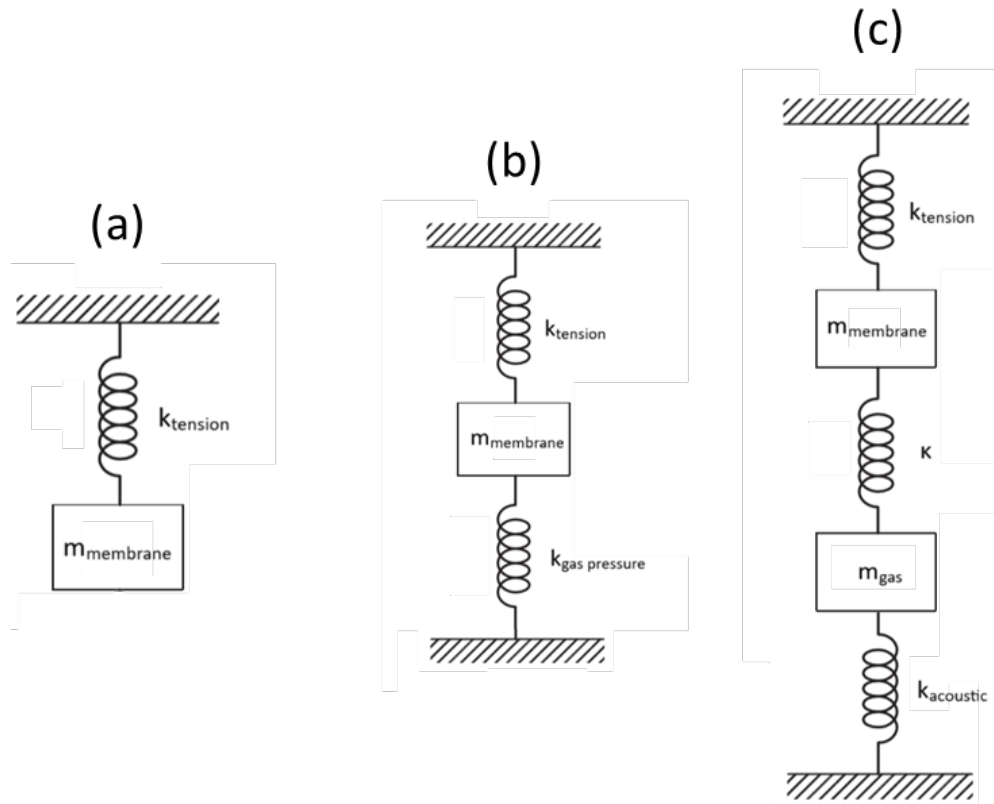


Figure 20 Modeling the three mechanisms affecting membrane vibrations using mass-spring harmonic oscillators. a) The first mechanism involves tension induced in the membrane; this tension, combined with the initial tension, is represented as a spring with spring constant  $k_{tension}$ . b) The gas within the cavity behaves like a spring, influencing membrane vibrations. c) The third model integrates the spring-like behavior of the gas with the acoustic vibration of the gas cavity, represented by  $k_{acoustic}$ .

In this chapter, three COMSOL models are developed to study the impact of these mechanisms on membrane vibrations. Section 4.3 details a model investigating the first mechanism, while Sections 4.4 and 4.5 describe models that explore the second and third mechanisms, respectively.

## 4.2 Model configuration

Informed by the experimental setup detailed in Yousefi's Ph.D. dissertation<sup>42</sup>, my COMSOL simulations aimed to replicate the conditions under which the MoS<sub>2</sub> membranes were tested. These membranes, suspended over a silicon oxide substrate, exhibit distinctive bulging behaviors in response to external pressure changes due to their impermeability and ability to trap pressure.

The dimensions and properties of membrane and gas cavity are summarized in table 11 and table 12.

Parameter	Value
Density	5060 kg/m <sup>3</sup>
2D Young's Modulus	128 N/m
Poisson's Ratio	0.29
Thickness	6.5 Å
Diameter	5 µm

Table 11 Dimensions and properties of suspended clamped MoS<sub>2</sub> membrane in pressurized membrane models.

Parameter	Value
Speed of Sound	323 m/s
Density	1.784 kg/m <sup>3</sup>
Specific gas constant	208.13 J/(kg.K)
Depth	1 µm
Diameter	5 µm

Table 12 Dimensions and properties of argon gas cavity in pressurized membrane models, at 298K.

Figure 21 illustrates the natural frequencies of the MoS<sub>2</sub> membrane pressurized with argon gas as a function of the external pressure in Yousefi's experiments. Notably, the frequency reaches its minimum value at an external pressure of approximately 10 kPa, indicating that the gas cavity pressure is also 10 kPa and there appear to be 2 modes of vibration visible with slightly different dispersion with pressure.

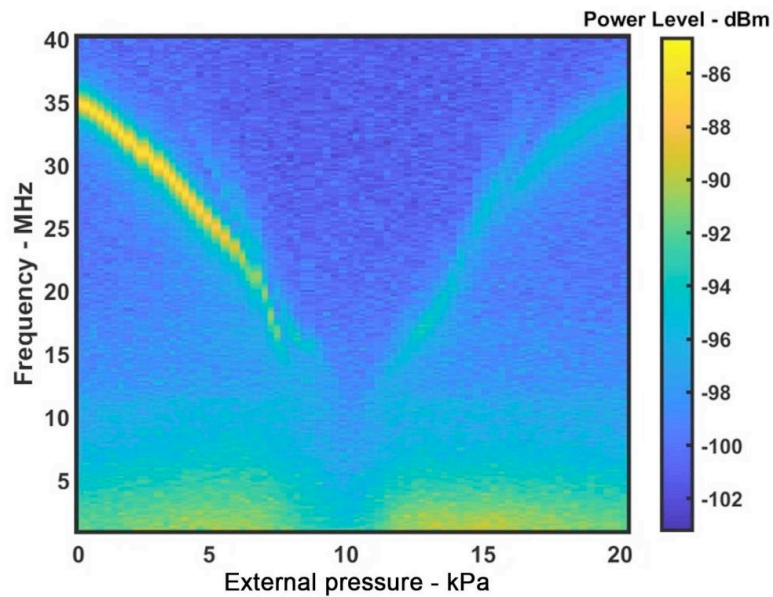


Figure 21 Experimental data showing the resonance frequency of a membrane with gas trapped beneath it<sup>42</sup> (Figure taken from; Yousefi).

### 4.3 Tension induced by gas pressure

To initiate the simulations, I first created a COMSOL model featuring a membrane subjected to uniform pressure. This section aims to explore the vibration of the MoS<sub>2</sub> membrane, focusing on its initial tension when flat and the additional tension arising from applied pressure. The pressure differential applied across the membrane, reflecting findings from Yousefi's experimental studies, ranges from -10 kPa to +10 kPa<sup>42</sup>.

For this simulation, I utilized the 3D interface in COMSOL. Adopting a procedure similar to the membrane simulation outlined in the preceding chapter, I initiated by establishing a work plane, upon which I drew a circle to represent the membrane's geometry. Within the membrane physics settings, I specified the initial tension using the initial stress and strain features. The boundary conditions were set to enforce a fixed constraint along the circular membrane's perimeter. To simulate the effect of gas pressure on the membrane, I applied a uniform face load across its surface, denoted by the pressure parameter  $P$ . Following the setup, I utilized a triangular mesh for discretization and conducted a parametric sweep within the eigenfrequency study, varying the pressure,  $P$ , from -10 kPa to +10 kPa.

The fundamental frequency of a membrane with tension resulting from deformation can be determined using Hencky's solution. The deformation of the membrane under a uniform net pressure  $\Delta P$  is calculated as follows:

$$\delta = C_2 \left( \frac{\Delta P a^4}{E n t_0} \right)^{\frac{1}{3}} \quad (4.1)$$

Furthermore, the frequency of a membrane with a tension  $T$  can be calculated using the following equation:

$$f = \frac{2.4040}{(\pi d)} \sqrt{\frac{T}{\rho t}} \quad (4.2)$$

In this equation,  $T$ , represents the total tension in the membrane, encompassing both the initial tension,  $T_0$ , and the tension induced by deformation, expressed as  $\frac{\Delta P a^2}{4\delta}$ . Therefore,

the fundamental frequency of the membrane, considering changes due to tensions, can be calculated as follows:

$$f = \frac{2.4048}{2\pi a} \sqrt{\frac{T_0 + \frac{\Delta P a^2}{4\delta}}{\rho_A}} \quad (4.3)$$

The results of this simulation, along with the theoretical frequencies derived from Hencky's solution, are displayed in Figure 22. Consistent with expectations<sup>50</sup>, the frequency exhibits a nonlinear response to the alterations in pressure.

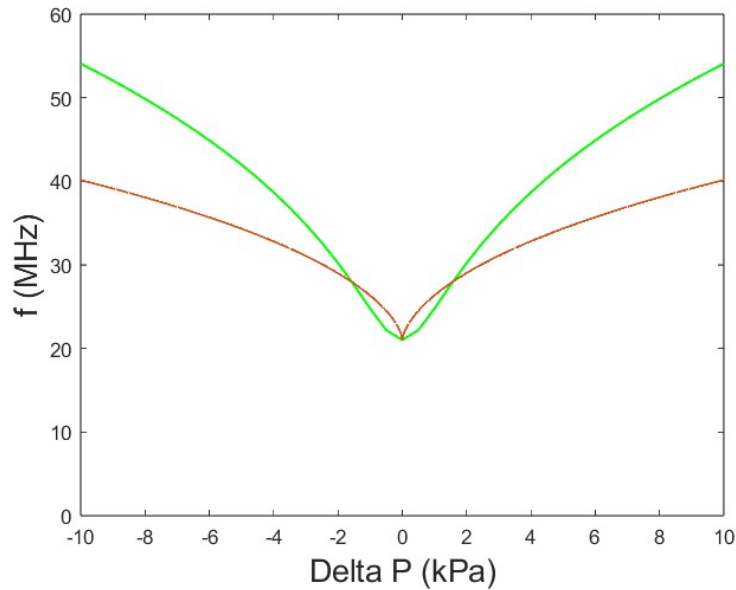


Figure 22 Fundamental natural frequency of the MoS<sub>2</sub> membrane as a function of the pressure difference applied across it, accounting only for the tension induced in the membrane based on the deformation. The green curve shows the simulation result while red curve represents theoretical model based on Hencky's solution (Eq. 4.3). The MoS<sub>2</sub> membrane features a diameter of 5 μm and a thickness of 6.5 Å.

While this model provides valuable insights into the natural frequencies of a pressurized membrane, its accuracy is limited. Subsequent sections of this chapter will

introduce COMSOL models for the spring characteristic of the gas pressure and the resonance of the coupled acoustic-membrane system for more precise analysis.

#### 4.4 Gas cavity modeled as a spring

In this section, we investigate the second mechanism by incorporating a spring foundation into the COMSOL model, positioned at the bottom surface of the membrane. To determine the stiffness of this spring, we consider a cylinder containing gas at pressure  $P$ . As the piston moves up and down within this cylinder, the force exerted by the gas on the piston can be calculated as follows:

$$F = A\Delta P \quad (4.4)$$

in which  $A$  represents the area of the piston and  $\Delta P$  denotes the changes in the pressure of the gas. If we consider the gas as a spring, the force exerted on the piston can be expressed as follows:

$$F = K_{Gas}\Delta h \quad (4.5)$$

Therefore, by equating these two expressions, we can determine the stiffness of the gas spring:

$$K_{Gas} = \frac{A\Delta P}{\Delta h} \quad (4.6)$$

For an ideal gas, the following relationship holds:

$$PV = nRT \quad (4.7)$$



$$\Delta P = \frac{dP}{dV} \Delta V = \frac{nRT}{V^2} \Delta V = \frac{P \Delta V}{V} \quad (4.8)$$

By substituting  $\Delta P$  from Equation 4.8 into Equation 4.6, we can calculate the value for  $K_{gas}$ :

$$K_{gas} = \frac{AP}{h} \quad (4.9)$$

In our model, with a diameter  $D = 5\mu m$ , height  $h = 1\mu m$ , and pressure  $P = 10 kPa$ , the calculated stiffness of the gas is  $K_{gas} = 0.196 N/m$ . Utilizing this stiffness value in the COMSOL model allows for the computation of the fundamental frequency of the membrane. The frequencies calculated in COMSOL and those derived from the theoretical energy method proposed by Yousefi (Equation 2.42) are both illustrated in Figure 23.

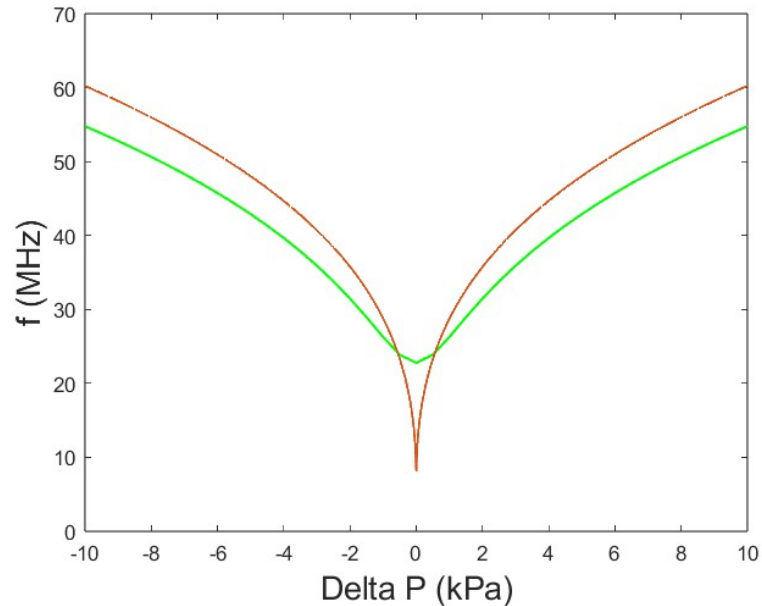


Figure 23 Fundamental natural frequency of the MoS<sub>2</sub> membrane as a function of the pressure difference applied across it, in the model with modeling gas as a spring. green curve shows the simulation result while red curve represents theoretical model based on energy method solution (Eq. 2.42). The MoS<sub>2</sub> membrane features a diameter of 5  $\mu m$  and a thickness of 6.5  $\text{\AA}$ .

## 4.5 Coupling between membrane vibration and acoustic resonance

### 4.5.1 *Acoustic resonance of gas cavity*

Acoustic resonance occurs when an object or cavity vibrates in reaction to an external sound wave at specific frequencies. These resonance frequencies depend on the physical dimensions, shape, and composition of the cavity. When a sound wave at one of these frequencies strikes the object, it causes the object to vibrate much more strongly than at other frequencies. This is due to the constructive interference of the waves reflected within or around the object, amplifying the vibration at the resonant frequency. Acoustic resonance can be observed in various contexts, such as musical instruments (e.g., the sound box of a guitar) and architectural acoustics (e.g., the reverberation of sound in a concert hall).

In this section, I developed a COMSOL model to determine the natural acoustic frequencies of an Argon gas cavity. In this simulation, the Pressure Acoustic physics interface within the Acoustics module of COMSOL was employed, alongside an eigenfrequency study, to determine the acoustic resonance frequencies of the gas cavity.

Table 13 lists the natural frequencies and corresponding mode shapes for the acoustic resonance of the cavity. The dimensions of the cavity are designed with a diameter of 5  $\mu\text{m}$  and a depth of 1  $\mu\text{m}$ .

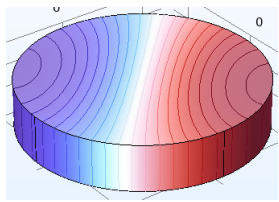
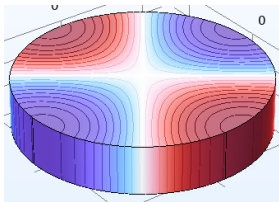
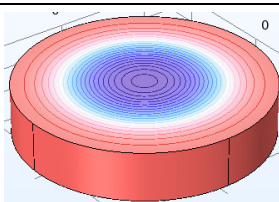
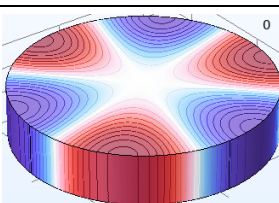
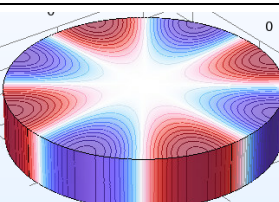
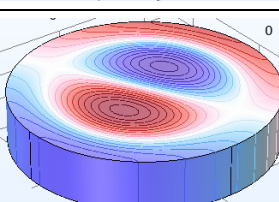
Mode Index (m,n)	Mode Shape	Frequency (MHz)
(1,1)		37.31
(2,1)		61.89
(0,2)		77.65
(3,1)		85.13
(4,1)		107.76
(1,2)		108.04

Table 13 Mode shapes and natural frequencies of acoustic resonance for the cylindrical gas cavity.

Theoretically, eigenfrequencies of gas cavity can be calculated using the Helmholtz equation in cylindrical coordinates, resulting in the following expression<sup>51</sup>:

$$f_{m,n,l} = \frac{v_{gas}}{2\pi} \sqrt{\left(\frac{\alpha_{m,n}}{R}\right)^2 + \left(\frac{l\pi}{2R}\right)^2} \quad (4.10)$$

Where  $c$  represents the speed of sound,  $R$  is the radius of the cylindrical cavity,  $\alpha_{m,n}$  is the  $n^{\text{th}}$  zero of the  $m^{\text{th}}$  order Bessel function, and  $m$ ,  $n$ , and  $l$  are the mode indices in the circumferential, radial, and longitudinal directions, respectively.

Generally, the acoustic resonance within a gas cavity is influenced by the speed of sound, which is determined by the formula:  $v_{gas} = \sqrt{\frac{\gamma P}{\rho}}$ , indicating its dependency on the gas pressure. Nonetheless, in the context of ideal gases, the speed of sound is given by:  $c = \sqrt{\gamma RT}$ , showing that it does not depend on pressure.

#### 4.5.2 Coupled acoustic-membrane simulation

To explore the interaction between the MoS<sub>2</sub> membrane and the Argon gas cavity, a comprehensive COMSOL model was developed. This model employs membrane physics for the MoS<sub>2</sub> layer and pressure acoustics physics for the Argon gas.

To define the geometry, a cylinder with a 1  $\mu\text{m}$  height and 5  $\mu\text{m}$  diameter is created in COMSOL to represent the entire system. This cylinder serves dual purposes: its volume models the argon gas using pressure acoustics physics, and its upper boundary models the MoS<sub>2</sub> membrane. The setup for boundary conditions, initial stress, and membrane thickness is consistent with previous models discussed in this thesis. A uniform face load

on the membrane simulates the net pressure. In pressure acoustics physics, the fluid model is set to be linear elastic and absolute pressure and initial pressure of the gas defined as 10 kPa, based on Yousefi's experimental results<sup>42</sup>.

The simulation incorporates a deforming domain over the cylinder within the definitions tab, enhancing the model's accuracy by accounting for fluid deformation. This is complemented by setting mesh smoothing to Laplace. Additionally, the membrane's interface with the gas is defined as an acoustic-structure boundary in the Multiphysics settings, enabling interaction between mechanical vibrations and acoustic pressures.

A stationary study setup was utilized to model the effect of external pressure on the membrane, while an eigenfrequency study, with considering geometric nonlinearity, was conducted to identify the coupled natural frequencies and their associated mode shapes.

Figure 26 presents the variation of the natural frequency of the MoS<sub>2</sub> membrane's first mode within the coupled system, demonstrating how it shifts with changes in pressure difference across the membrane, ranging from -10 kPa to +10 kPa.

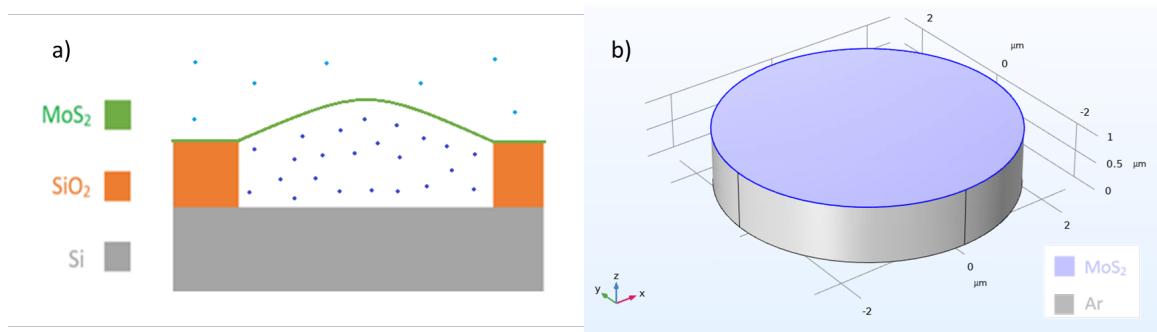


Figure 24 Schematic of the experimental geometry (side view). b) Simulation geometry in COMSOL.

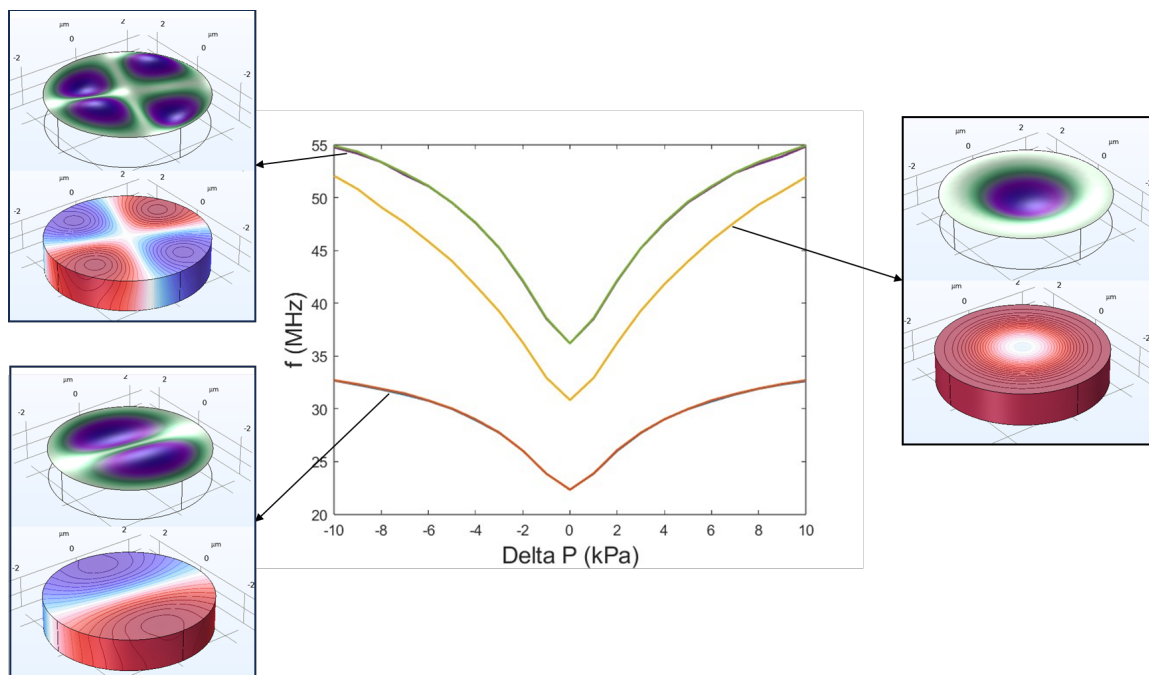


Figure 25 Resonance modes of the coupled acoustic-membrane system featuring the first three modes. The yellow curve, marked by distinct mode shapes and notable sensitivity to pressure fluctuations, represents the MoS<sub>2</sub> mode within this system. The membrane is a single-layer MoS<sub>2</sub> with a 6.5 Å thickness and 5 μm diameter. The cavity is modeled as a cylinder, also with a 5 μm diameter and a depth of 1 μm.

Figure 25 reveals that the direction of the net pressure has minimal impact on the system's natural frequency, a finding consistent with experimental observations<sup>42</sup> (Figure 21). We anticipated, to see both the acoustic resonance modes and the natural frequencies of MoS<sub>2</sub> within the hybridized modes in the acoustic-membrane coupled system<sup>52,53</sup>. Considering the mode shapes and how frequencies respond to changes in net pressure applied to the membrane, the yellow curve in Figure 25 represents the first mode of the MoS<sub>2</sub> membrane in the coupled system and two other curves in the figure represent the acoustic modes in the coupled system.

Comparing simulation results for a pressurized membrane without acoustic considerations (previously depicted as the green curve in Figure 22) with those of the

membrane coupled to argon gas's acoustic resonance (shown in Figure 25) reveals significant insights. Figure 26 compares the first mode of MoS<sub>2</sub> in both scenarios, demonstrating how acoustic coupling affects the membrane's eigenfrequency. This effect is being observed because the acoustic resonance frequency of the Argon gas cavity, as explored in Table 13, matches the MHz range of the membrane's natural frequency. When the acoustic resonance closely aligns with the membrane's natural frequency, the coupling between the membrane and the acoustic environment intensifies<sup>52</sup>.

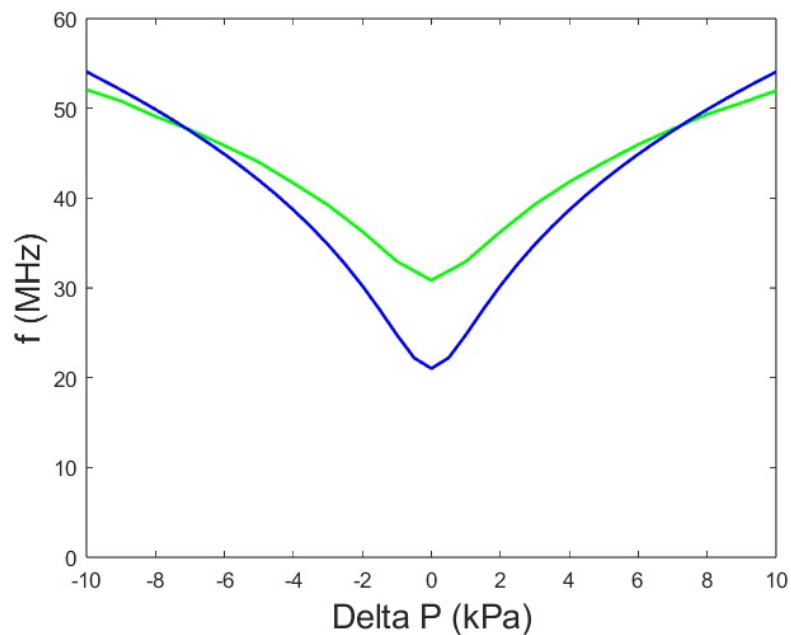


Figure 26 Simulation results of the first mode frequency of a pressurized MoS<sub>2</sub> membrane: the green curve represents the membrane coupled with the acoustic resonance of the gas cavity, and the blue curve represents the membrane without acoustic coupling. The membrane has a diameter of 5  $\mu\text{m}$ , and the gas cavity beneath it has a depth of 1  $\mu\text{m}$ .

## 4.6 Conclusion

This chapter is dedicated into the Finite Element modeling of pressurized MoS<sub>2</sub> membranes, a vital exploration of how two-dimensional materials respond under stress, offering insights valuable for applications like pressure sensors. Through COMSOL simulations, we have advanced the understanding of pressurized membrane dynamics, initially by focusing on the MoS<sub>2</sub> membrane's response to uniform pressure. Subsequently, we expanded our investigation to cover the acoustic resonance of argon gas and the complex interaction between mechanical and acoustic resonances within a coupled system. By simulating these phenomena, we are able to observe the expected behaviors of MoS<sub>2</sub> and acoustic modes in the hybridized system. The chapter concludes with a closer examination of the coupled system, validating the simulation's alignment with a previously established model.

Overall, this investigation not only confirms theoretical predictions but also enhances our comprehension of the dynamic interactions within coupled acoustic-membrane systems. The findings facilitate further research into optimizing these systems for practical NEMS pressure sensing applications.



## CHAPTER 5. CONCLUSION

### 5.1 Summary

In this thesis, we explored the dynamic behaviors and vibrational characteristics of nanoelectromechanical systems (NEMS), focusing on two primary aspects: the coupling of MoS<sub>2</sub> membranes with SiN<sub>x</sub> drumheads and the influence of gas pressure on the vibrational properties of MoS<sub>2</sub> membranes. Through extensive finite element simulations and theoretical model development, we sought to enhance the understanding of these systems for the advancement of NEMS device technology.

The first part of our investigation detailed the finite element simulations of the coupled MoS<sub>2</sub> membrane and SiN<sub>x</sub> drumhead system, revealing complex mechanical behaviors and vibrational characteristics. Our work extended to calculating the coupling constants between different modes of the coupled system, providing insights into their interactive dynamics. This analysis not only filled existing research gaps but also laid a foundation for optimizing nanomechanical systems design.

Subsequently, we turned our attention to the effects of gas pressure on MoS<sub>2</sub> membranes. By simulating the pressurized membrane's response and its interaction with Argon gas, we identified key vibrational behaviors that align with theoretical predictions. These findings contribute to a deeper understanding of pressurized membrane dynamics, necessary for the development of high-sensitivity NEMS-based pressure sensors.

Overall, this thesis contributes valuable insights into the vibrational dynamics of coupled nanoresonators and pressurized membranes, paving the way for future innovations in the field of NEMS devices.

## **5.2 Future outlook**

The exploration started in this thesis opens numerous openings for future research and development in the field of nanoelectromechanical systems (NEMS). Several key areas promise to further our understanding and application of NEMS devices, particularly those incorporating MoS<sub>2</sub> membranes.

### *Application Development*

The fundamental insights gained from this thesis could be translated into real-world applications, from highly sensitive sensors capable of detecting minute forces or chemical species, to high-frequency resonators for signal processing or energy harvesting devices. Modifying the design and fabrication of NEMS devices to specific applications will be crucial for their successful integration into commercial products.

### *Multi-Resonator Systems*

Expanding the study to systems incorporating multiple coupled resonators to form complex NEMS arrays. Such systems could lead to novel computing paradigms and ultra-sensitive sensor arrays capable of detecting a broader range of physical or chemical stimuli.

### *Improving Simulation Models and Theoretical Understanding*

Enhancing simulation models to include effects such as thermal fluctuations, material anisotropy, and non-linear dynamics could improve the predictive power of simulations and lead to a deeper understanding of NEMS behavior under real-world conditions.

## BIBLIOGRAPHY

1. Sharma, M., Sathyadharma Prasad, A., Freitag, N. H., Büchner, B. & Mühl, T. Coupled mechanical oscillator enables precise detection of nanowire flexural vibrations. *Communications Physics* **6**, (2023).
2. Carter, B. *et al.* Coupled Nanomechanical Graphene Resonators: A Promising Platform for Scalable NEMS Networks. *Micromachines* **14**, 1–12 (2023).
3. Dolleman, R. J. *et al.* Squeeze-Film Effect on Atomically Thin Resonators in the High-Pressure Limit. *Nano Letters* **21**, 7617–7624 (2021).
4. Craighead, H. G. Nanoelectromechanical Systems. *Science*. **290**, 399–420 (2000).
5. Li, Y. *et al.* The Oral Fluid MEMS/NEMS Chip (OFMNC): diagnostic and translational applications. *Advances in Dental Research* **18**, 3–5 at <https://doi.org/10.1177/154407370501800102> (2005).
6. Roukes, M. Nanoelectromechanical systems face the future. *Physics World* **14**(2), 25 (2001). <https://iopscience.iop.org/article/10.1088/2058-7058/14/2/29/pdf>
7. Ekinici, K. L. & Roukes, M. L. Nanoelectromechanical systems. *Review of Scientific Instruments* **76**, 1–12 (2005).
8. Carr, D. W., Sekaric, L. & Craighead, H. G. Measurement of nanomechanical resonant structures in single-crystal silicon. *Journal of Vacuum Science & Technology. B, Microelectronics and Nanometer Structures: Processing, Measurement, and Phenomena*. **16**, 3821–3824 (1998).
9. Espinosa, H. D., Ke, C. & Pugno, N. Nanoelectromechanical Systems: Experiments and Modeling. *Encyclopedia of Materials: Science and Technology* vol. 1 (2006).
10. Lembke, D., Bertolazzi, S. & Kis, A. Single-Layer MoS<sub>2</sub> Electronics. *Accounts of Chemical Research* **48**, 100–110 (2015). <https://doi.org/10.1021/ar500274q>
11. K.S. Novoselov, A.K. Geim, S.V. Morozov, D. Jiang, Y. Zhang, S.V. Dubonos, I.V. Grigorieva, A. A. Firsov. Electric Field Effect in Atomically Thin Carbon Films. *Science* **306**(5696), 666–669 (2004). <https://doi.org/10.1126/science.1102896>
12. Bunch, J. S. *et al.* Electromechanical resonators from graphene sheets. *Science* **315**, 490–493 (2007).
13. Novoselov, K. S. *et al.* A roadmap for graphene. *Nature* **490**, 192–200 (2012).

14. Raccichini, R., Varzi, A., Passerini, S. & Scrosati, B. The role of graphene for electrochemical energy storage. *Nature Materials* **14**, 271–279 (2015).
15. Dubey, N. *et al.* Graphene: A Versatile Carbon-Based Material for Bone Tissue Engineering. *Stem Cells International* **2015**, 18–23 (2015).
16. Radisavljevic, B., Radenovic, A., Brivio, J., Giacometti, V. & Kis, A. Single-layer MoS<sub>2</sub> transistors. *Nature Nanotechnology* **6**, 147–150 (2011).
17. Lee, W. *et al.* Two-dimensional materials in functional three-dimensional architectures with applications in photodetection and imaging. *Nature Communications* **9**, 1–9 (2018).
18. Wang, Q. H., Kalantar-Zadeh, K., Kis, A., Coleman, J. N. & Strano, M. S. Electronics and optoelectronics of two-dimensional transition metal dichalcogenides. *Nature Nanotechnology* **7**, 699–712 (2012).
19. Mak, K. F. & Shan, J. Photonics and optoelectronics of 2D semiconductor transition metal dichalcogenides. *Nature Photonics* **10**, 216–226 (2016).
20. Liu, H., Du, Y., Deng, Y. & Ye, P. D. Semiconducting black phosphorus: Synthesis, transport properties and electronic applications. *Chemical Society Reviews* **44**, 2732–2743 (2015).
21. Huang, Y. *et al.* Reliable Exfoliation of Large-Area High-Quality Flakes of Graphene and Other Two-Dimensional Materials. *ACS Nano* **9**, 10612–10620 (2015).
22. Zhang, Y. I., Zhang, L. & Zhou, C. Graphene and Related Applications. *Accounts of Chemical Research* **46**, 2329–2339 (2013).
23. Lemme, M. C. *et al.* Nanoelectromechanical Sensors Based on Suspended 2D Materials. *Research: A Science Partner Journal* **2020**, 8748602 (2020). <https://doi.org/10.34133/2020/8748602>
24. Zhang, P. *et al.* Nanoelectromechanical Memories Based on Nonlinear 2D MoS<sub>2</sub> Resonators. *Proceedings. IEEE International Conference on Micro Electro Mechanical Systems*. **2022**, 208–211 (2022). doi: 10.1109/MEMS51670.2022.9699463.
25. Feng, P. X. L. *et al.* Two-dimensional nanoelectromechanical systems (2D NEMS) via atomically-thin semiconducting crystals vibrating at radio frequencies. *2014 IEEE International Electron Devices Meeting*, pp. 8.1.1-8.1.4, doi: 10.1109/IEDM.2014.7047008

26. Manzeli, S., Dumcenco, D., Migliato Marega, G. & Kis, A. Self-sensing, tunable monolayer MoS<sub>2</sub> nanoelectromechanical resonators. *Nature Communications* **10**, 1–8 (2019).
27. Lee, J., Wang, Z., He, K., Shan, J. & Feng, P. X. L. High frequency MoS<sub>2</sub> nanomechanical resonators. *ACS Nano* **7**, 6086–6091 (2013).
28. Jiang, J. W. Graphene versus MoS<sub>2</sub>: A short review. *Frontiers in Physics* **10**, 287–302 (2015).
29. Venkata Subbaiah, Y. P., Saji, K. J. & Tiwari, A. Atomically Thin MoS<sub>2</sub>: A Versatile Nongraphene 2D Material. *Advanced Functional Materials* **26**, 2046–2069 (2016).
30. Chhowalla, M. *et al.* The chemistry of two-dimensional layered transition metal dichalcogenide nanosheets. *Nature Chemistry* **5**, 263–275 (2013).
31. Devi, R., Singh Gill, S. & Singh, B. Low-pressure NEMS sensor design with slotted squared diaphragm structure. *Materials Today. Proceedings* **74**, 186–189 (2021).
32. Rao, S. S. *Vibration of Continuous Systems*. (2019). John Wiley & Sons, Inc.
33. Schmid, S., Villanueva, L. G. & Roukes, M. L. *Fundamentals of Nanomechanical Resonators*. (2016). Springer Cham.
34. Zande, A. M. Van Der *et al.* Large-Scale Arrays of Single-Layer Graphene. *Nano Letters* **10**(12), 4869–4873 (2010) doi:10.1021/nl102713c
35. Xu, B. *et al.* Nanomechanical Resonators : Toward Atomic Scale. *ACS Nano* **16**(1), (2022) doi:10.1021/acsnano.2c01673
36. Hauer, B. D., Doolin, C., Beach, K. S. D. & Davis, J. P. A general procedure for thermomechanical calibration of nano/micro-mechanical resonators. *Annals of Physics* **339**, 181–207 (2013). <https://doi.org/10.1016/j.aop.2013.08.003>
37. Tornabene, F., Viola, E. & Inman, D. J. 2-D differential quadrature solution for vibration analysis of functionally graded conical, cylindrical shell and annul plate structures. *Journal of Sound and Vibration* **328**, 259–290 (2009).
38. Anetsberger, G. *et al.* Near-field cavity optomechanics with nanomechanical oscillators. *Nature Physics* **5**(12), 909–914 (2009).
39. Schwarz, C. *et al.* Deviation from the Normal Mode Expansion in a Coupled Graphene-Nanomechanical System. *Physical Review Applied* **6**, 1–6 (2016).

40. Faust, T., Rieger, J., Seitner, M. J., Kotthaus, J. P. & Weig, E. M. Coherent control of a classical nanomechanical two-level system. *Nature Physics* **9**, (2013).
41. Novotny, L. Strong coupling, energy splitting, and level crossings: A classical perspective. *American Journal of Physics* **78**, 1199–1202 (2010).
42. Yousefi, F. S. Dynamics of MoS2 Resonators Coupled to Acoustic and Mechanical Systems. Doctoral dissertation – Boston University (2024).
43. Fichter, W. B. Some Solutions for the Large Deflections of Uniformly Loaded Circular Membranes. *NASA Technical Paper* **3658**, (1997).  
<https://ntrs.nasa.gov/api/citations/19970023537/downloads/19970023537.pdf>
44. Lloyd, D. *et al.* Supporting Information to "Adhesion, Stiffness and Instability in Atomically Thin MoS2 Bubbles." *Nano Letters* **17**(9), 5329–5334.  
<https://doi.org/10.1021/acs.nanolett.7b01735>
45. Boddeti, N. G. *et al.* Mechanics of adhered, pressurized graphene blisters. *Journal of Applied Mechanics* **80**(4), 040909 (2013). <https://doi.org/10.1115/1.4024255>
46. Zienkiewicz, O. C., Taylor, R. L. & Zhu, J. Z. *The Finite Element Method: Its Basis and Fundamentals*. Sixth edition. (2005). Butterworth Heinemann.
47. Faust, T. *et al.* Nonadiabatic dynamics of two strongly coupled nanomechanical resonator modes. *Physical Review Letters* **109**, 037205 (2012).  
<https://doi.org/10.1103/PhysRevLett.109.037205>
48. Liu, C. H., Kim, I. S. & Lauhon, L. J. Optical Control of Mechanical Mode-Coupling within a MoS2 Resonator in the Strong-Coupling Regime. *Nano Letters*. **15**, 6727–6731 (2015).
49. Lloyd, D. *et al.* Adhesion, Stiffness, and Instability in Atomically Thin MoS2 Bubbles. *Nano Letters* **17**, 5329–5334 (2017).
50. Sarafraz, A. *et al.* Pressure-induced nonlinear resonance frequency changes for extracting Young's modulus of nanodrums. *Nonlinear Dynamics* **111**, 14751–14761 (2023).
51. Rona, A. The acoustic resonance of rectangular and cylindrical cavities. *Journal of Algorithms & Computational Technology* **1**(3), 329–356 (2007).  
<https://doi.org/10.1260/174830107782424110>
52. Gorman, D. G., Reese, J. M., Horáček, J. & Dedouch, K. Vibration analysis of a circular disc backed by a cylindrical cavity. *Proceedings of the Institution of Mechanical Engineers. Part C. Journal of Mechanical Engineering Science* **215**,

1303–1312 (2001).

53. Rajalingham, C., Bhat, R. B. & Xistris, G. D. Vibration of circular membrane backed by cylindrical cavity. *International Journal of Mechanical Sciences* **40** 723–734 at [https://doi.org/10.1016/S0020-7403\(97\)00065-9](https://doi.org/10.1016/S0020-7403(97)00065-9) (1998).
54. Greywall, D. S., Busch, P. A. & Walker, J. A. Phenomenological model for gas-damping of micromechanical structures. *Sensors and Actuators* 72(1), 49–70 (1999). [https://doi.org/10.1016/S0924-4247\(98\)00203-9](https://doi.org/10.1016/S0924-4247(98)00203-9)



## CURRICULUM VITAE

